Oceanologia, uncorrected, in press
Polish Academy of Sciences
Institute of Oceanology

https://doi.org/10.5697/...

Seasonal and spatial variability of Fluorescent Dissolved Organic Matter in the southern Baltic Sea

Monika Zabłocka*, Piotr Kowalczuk, Aleksandra Winogradow, Karol Kuliński

Abstract

This study presents a comprehensive analysis of Fluorescent (FDOM) and Chromophoric (CDOM) Dissolved Organic Matter in the southern Baltic Sea, enhancing our understanding of its composition, sources, and dynamics in a semi-enclosed marine system. The Baltic Sea's unique hydrography and strong freshwater inflow served as a natural laboratory for investigating interactions between terrestrial and marine Dissolved Organic Matter (DOM).

We examined spatial and seasonal variations of CDOM and FDOM, using absorption and fluorescence spectroscopy combined with parallel factor analysis (PARAFAC). Six fluorophore groups (C1–C6) were identified, with humic-like components (C1–C3, C5) of terrestrial and marine origin dominating the FDOM composition. Protein-like components (C4, C6) were more prominent in Open Waters (OW), particularly in late summer and fall. Humic-like fluorescence intensity (I_h) contributed 61–96% to total fluorescence (I_{tot}). The total fluorescence intensity was much higher in the Gulf and Coastal Waters, GCW than in the Open Waters (OW) of the Baltic Sea. The vertical distributions of FDOM varied by region. In the Open Baltic Deep Waters (OBDW) the highest I_h values were observed near the bottom, likely resulting from diffusion of DOM from sediments, and the lowest at the surface. In the Gulf of Gdańsk Deep Waters (GGDW) I_h was the lowest in the Baltic Sea Winter Water (BSWW). I_p was the highest at the surface and the weakest at the bottom, in both areas.

This study offers new insight into the spatial, seasonal, and vertical behavior of FDOM and underscores its sensitivity to environmental conditions.

Keywords

Fluorescent Dissolved Organic Matter (FDOM); Chromophoric Dissolved Organic Matter (CDOM); Gulf of Gdańsk; Parallel Factor Analysis (PARAFAC)

Institute of Oceanology, Polish Academy of Sciences, Sopot, Poland
***Correspondence**: monika_z@iopan.pl (M. Zabłocka)

Received: 2 April 2025; **revised:** 28 November 2025; **accepted**: 16 December 2025

1. Introduction

Dissolved Organic Matter (DOM) represents the largest reservoir of organic matter in marine environments, accounting for approximately 97% of the ocean's organic carbon, exceeding the carbon inventory contained within oceanic biomass by more than 200 times (Hansell et al., 2009). This carbon pool is comparable in magnitude to the amount of carbon contained within the Earth's atmosphere and terrestrial vegetation (Hansell and Carlson, 2001; Hansell, 2013; Friedlingstein et al., 2025). DOM is now understood as a heterogeneous continuum encompassing rapidly cycled labile fractions as well as long-lived refractory components with residence times of hundreds to thousands of years. Advances in analytical techniques have greatly improved our ability to resolve this continuum and to elucidate the transformation pathways linking labile and refractory DOM pools. Within this conceptual framework, the microbial carbon pump (MCP, Jiao et al., 2010, 2011) provides a mechanistic explanation of how microbial processes generate, transform, and sustain refractory DOM, thereby contributing to its long-term persistence in the ocean's interior. Recent analytical advances have highlighted the dynamic continuum between these pools. It is recognized that DOM plays an active and dynamic role in carbon sequestration through microbial processes (Løn-borg et al., 2020; Wagner et al., 2020). The vast majority of the ocean's organic matter originates from autochthonous production by photosynthetic autotrophic organisms in the surface ocean (with a small contribution of chemosyn-

thetic organisms within the ocean's interior), and serves as a substrate supporting vast heterotrophic prokaryote populations within the entire marine environment (Jiao et al., 2010; Hansell, 2013). Most of the autochthonous DOM is biogeochemically labile and quickly respired to CO_2. The terrestrial sources of DOM contribute to a relatively small portion (approximately 2–3%) of the oceanic DOM pool (Opsahl and Benner, 1997). However, this DOM fraction constitutes a significant component near ocean margins and semi-enclosed seas influenced by riverine outflows (Lønborg et al., 2024, 2025).

Chromophoric dissolved organic matter (CDOM), the fraction of DOM that interacts with light, significantly influences the optical properties of natural waters. The CDOM absorption spectrum is monotonic, featureless and decreases exponentially with increasing wavelengths (Jerlov, 1976). On a global scale, the mean relative contribution of CDOM to the total absorption coefficient of seawater exceeds 70% in the UV-A spectral range, and decreases sharply to negligible values in the red spectral range (< 550 nm) (Nelson and Siegel, 2013). CDOM directly impacts the penetration and spectral quality of light in the water column, thereby influencing vertical heat distribution and indirectly affecting key processes such as primary production, thermal stratification, and the exposure of marine life to ultraviolet radiation (Babin et al., 2003; Cahill et al., 2023). The global distribution of the CDOM absorption coefficient at 325 nm, $a_{\mathrm{CDOM}}(325)$, in surface waters shows a distinct spatial pattern, with minimum values in the subtropical gyres of the Atlantic, Pacific, and Indian Oceans, and maximum values in the North Atlantic and North Pacific (Nelson and Siegel, 2013). This spatial variability likely reflects differences in the age of water mass, the ventilation rates, and the sources of CDOM. For example, concentrations increase with depth, as photobleaching is largely limited to the surface layer, especially in the subtropical gyres. In contrast, deep waters, especially of the Northern Pacific, contain higher levels of CDOM due to the longer residence time of these waters and the lower ventilation rates. $a_{\mathrm{CDOM}}(325)$ is significantly correlated with apparent oxygen utilization (AOU) in the deep Pacific and Indian Oceans. This relationship suggests microbial production of CDOM in the ocean interior, where oxygen consumption by microbial respiration contributes to CDOM accumulation (Nelson et al., 2010). The global CDOM distribution points toward dynamic equilibrium between its production, via, e.g., microbial activity in the deep ocean or decaying phytoplankton biomass in surface waters – and its photochemical degradation in the surface mixed layer (Nelson et al., 2010; Nelson and Siegel, 2013). In continental margins and shelf seas, the inflow of freshwater, along with its dilution and mixing with the adjacent marine water, further regulates CDOM concentrations in these areas (Stedmon et al., 2010; Stedmon and Nelson, 2015).

A fraction of CDOM, called Fluorescent Dissolved Organic Matter (FDOM), has the inherent ability to emit a fraction of the absorbed energy as fluorescence. A fluorescence spectroscopy technique called the Excitation Emission Matrix (EEM), which involves measurements of emission spectra at a series of successively increasing excitation wavelengths, enabled the identification of local fluorescence intensity maxima occurring within characteristic excitation and emission wavelength ranges that could be assigned to broad classes of dissolved organic compounds constituting DOM (Coble, 1996). This technique has significantly improved our understanding of the complex characteristics of FDOM by allowing the classification of various fluorophores based on their distinct excitation and emission peaks, which can be linked to terrestrial, marine, or anthropogenic sources (Stedmon et al., 2003). The application of the multivariate statistical method, called Parallel Factor Analysis (PARAFAC), for the objective interpretation of EEM spectra has significantly broadened our ability to analyze these complex data sets, providing valuable insights into DOM production, degradation, and distribution in various marine environments (Jørgensen et al., 2011; Kowalczuk et al., 2013; Catalá et al., 2016; Zabłocka et al., 2025).

The Baltic Sea is a shallow, semi-enclosed sea with limited water exchange and high freshwater input, leading to elevated concentrations of C/FDOM and a complex interaction of physical and biogeochemical processes that significantly influence its optical propert ies (Simis et al., 2017; Kratzer and Moore, 2018). Although there are studies characterizing FDOM in the Baltic Sea water column (Kowalczuk et al., 2005b), near bottom waters (Reader et al., 2019), surface microlayer (Drozdowska, 2007a,b; Drozdowska et al., 2018), and sea ice (Stedmon et al., 2007), there is a lack of empirical studies on the temporal and spatial variability of the qualitative and quantitative composition of FDOM, based on fluorescence spectroscopy and multivariate statistical methods. This was the motivation for the present study, which aimed to investigate historical, high-quality data sets containing original data collected during multiyear hydrographic surveys conducted by the Institute of Oceanology in the Baltic Sea between 2008–2013. The primary objectives of this research are: (i) assess the composition of fluorescent dissolved organic matter (FDOM) in distinct marine basins of the southern Baltic Sea, using fluorescence spectroscopy and multivariate statistical analysis (PARAFAC); (ii) characterize the spatial variability of identified components at horizontal and vertical dimension; (iii) evaluate the seasonal cycles of identified FDOM components and calculated spectral indices; (iv) examine the compositional transformation of FDOM based on the distribution of spectral indices in distinct water masses; (v) investigate the spatial and seasonal variability of chromophoric dissolved organic matter (CDOM), including absorption coefficients, spectral slope coefficients and SUVA(254).

2. Material and methods

2.1 The study area

The Baltic Sea (Figure 1) is a shallow and geologically young semi-enclosed sea located in Northern Europe, connected to the North Sea via the shallow and narrow Danish Straits. Its extensive drainage area results in a high freshwater input, which, combined with limited water exchange with the North Sea, leads to elevated concentrations of Chromophoric Dissolved Organic Matter (CDOM). As a result, the optical properties of the Baltic Sea waters are highly influenced by the presence of riverine CDOM (Kowalczuk, 1999).

In the southern Baltic Sea, located within the temperate climatic zone, maximum freshwater inflow typically occurs in March and April (Figure S1) , coinciding with the spring phytoplankton bloom (Figure S2). River runoff (approximately 436 km^3 $year^{-1}$; Leppäranta and Myrberg, 2009) carries high loads of DOM (3–3.96 TgC $year^{-1}$) and inorganic nutrients, which fuel the spring bloom. During this period, light attenuation increases significantly. In spring and summer, a density boundary is formed at the thermocline layer, preventing the mixing of organic matter (OM)-rich surface water with water below the thermocline. In summer, the optical properties of Gulf and Coastal Waters are affected by periodic floods and local upwelling. In winter, absorption and attenuation decrease as a result of wind-driven vertical mixing, thermocline disappearance, small biological activity, and reduced river runoff (Sagan, 1991, 2008; Olszewski et al., 1992; Kowalczuk, 1999). The absence of thermal stratification allows the convective vertical mixing in the water column to depths of 60–80 meters (Leppäranta and Myrberg, 2009) where a permanent halocline – a strong physical boundary, is formed. The halocline inhibits vertical mixing between the oxygenated brackish surface layer (salinity of approximately 7–8), and the less oxygenated (or even anoxic) and saltier deeper waters (salinity ranging from 10 in northern Gotland to 22 in the Arkona Basin; Schmidt et al., 2021).

Below the halocline, absorption slowly increases toward the sea bottom in the blue to green spectral bands. The scattering, however, remains much higher compared to overlying waters above the halocline, due to the resuspension of particles from bottom sediments and sinking particulate matter produced in the euphotic zone during phytoplankton blooms (Sagan, 2008). Below the permanent halocline, a significant anomaly in CDOM distribution, characterized by its elevated absorption (Kowalczuk et al., 2015), was observed. One potential source of the elevated CDOM concentrations observed in deep waters is the release of dissolved organic matter from the sediments pore water into the overlying water (Reader et al., 2019; Loginova et al., 2024; Terzić et al., 2024).

2.2 Sample collection and processing

2.2.1 Sample collection

Water samples were collected during 27 cruises conducted over six consecutive years (2008–2013) on board the r/v *Oceania* – an Institute of Oceanology Polish Academy of Sciences (IO PAN) research vessel (Table S1). The water samples were collected mainly from the Baltic Proper (with the vast majority of samples collected in the southern part), Pomeranian Bay, Szczecin Lagoon, and Gulf of Finland (Figure 1, Table S1).

Water for all parameters was collected with a single 30-liter Niskin bottle deployed through the ship's winch system, into acid-washed 20 L canisters. Sampling depths were selected based on the vertical distribution of hydrological and biooptical properties in the water column (i.e., the thermohaline structure and phytoplankton abundance).

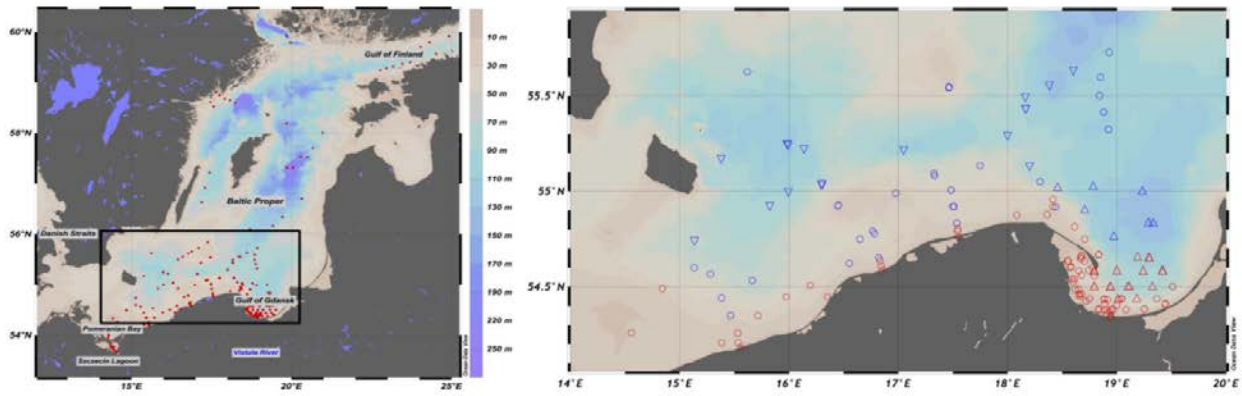

Figure 1. Location of sampling stations: left panel – all sampled stations, right panel – stations selected for detailed analysis; in red: GCD (Gulf of Gdańsk and Coastal Waters), in blue: OW (Open Waters), triangle: GGDW (Gulf of Gdansk Deep Waters), reversed triangle: OBDW (Open Baltic Deep Waters).

Water samples for CDOM, FDOM and DOC were collected mainly from: the surface, the middle of the mixed layer, the thermocline layer (if present), the subsurface chlorophyll *a* maximum (if present), below the halocline (if present), and near the seabed. The water samples for chlorophyll *a* concentration measurements were collected mainly from the surface water and from the maximum chlorophyll *a* depth.

At all stations, vertical profiles of temperature and salinity were measured with a Sea-Bird SBE 49 FastCAT CTD probe (Sea-Bird Electronics, USA).

2.2.2 Sample processing

The water samples collected for CDOM, FDOM, and DOC concentration measurements underwent a two-step filtration process. The seawater was first filtered through Whatman glass-fiber filters (GF/F, nominal pore size 0.7 μm) in order to remove large-size particles, and then through acid-washed Sartorius 0.2 μm pore size cellulose membrane filters, to remove fine-size particles. All samples were filtered into precombusted 40 mL amber glass vials and stored at 4°C in the dark, which preserves DOM optical properties for several weeks (Stedmon and Markager, 2001). Samples for DOC were additionally acidified with 150 μL 0.1 M HCl.

2.2.3 CDOM absorption measurements

CDOM absorption of water samples was measured with two spectrophotometers. In 2008–2010, spectral absorption was measured with a double-beam UNICAM UV4 100 spectrophotometer in the spectral range 200–700 nm with 1 nm resolution. In 2011–2013, spectral absorption was measured with a double-beam PerkinElmer Lambda 650 spectrophotometer in the spectral range 240–700 nm with 1 nm resolution. Two lengths of quartz cuvettes were used for the measurements: 0.05 m (UNICAM UV4 100) and 0.10 m (PerkinElmer Lambda 650). A comparison of measurements from both spectrophotometers showed consistent CDOM absorption values within the expected range of instrument precision. All absorbance spectra were blank-corrected using ultrapure water (Mili-Q) as a reference. A baseline correction was performed by subtracting the average absorbance in the 650–700 nm region to remove potential background offset. Measurements were conducted at room temperature.

The CDOM absorbance, $A(\lambda)$, spectra were transformed to the CDOM absorption coefficient, $a_{\mathrm{CDOM}}(\lambda)$, using the following equation:

$$a_{\mathrm{CDOM}}(\lambda) = 2.303\, A(\lambda)/l \quad (1)$$

where $A(\lambda)$ is the absorbance, l is the optical path length in meters and the factor 2.303 is the natural logarithm of 10.

The slope coefficients of the CDOM absorption spectra, $S_{300-600}$, were calculated for the 300–600 nm spectral range (Kowalczuk et al., 2015) from Equation (2):

$$a_{\mathrm{CDOM}}(\lambda) = a_{\mathrm{CDOM}}(\lambda_0)e^{-S(\lambda-\lambda_0)} + K \quad (2)$$

where λ_0 is 375 nm, and K is a background constant of the baseline shift resulting from the residual scattering by fine size particle fractions, micro-air bubbles or colloidal material present in the sample, refractive index differences between the sample and the reference, or attenuation not due to CDOM.

Equation (2) was implemented in the Matlab R2020 environment by adopting a nonlinear least-squares fit method (Stedmon et al., 2000; Kowalczuk et al., 2006), with the use of the Curve Fitting toolbox and the Trust Region algorithm.

2.2.4 DOM fluorescence measurements and the PARAFAC model

Fluorescent Excitation/Emission Matrices (EEM) of collected water samples were measured with a Varian Cary Eclipse spectrofluorometer in a 1 cm quartz cuvette. The excitation spectral range was 240–500 nm with a 5 nm increment. The emission signal was recorded in a 250-600 nm spectral range with a 2 nm increment. The monochromator measurement slots, for both excitation and emission, were set to 5 nm. The excitation energy of every sample was controlled by adjusting the electric voltage of the xenon lamp to avoid saturation of the emission signal. In general, the electric voltage on the xenon lamp was set at 1000 V and reduced to 900 or 800 V for samples rich in FDOM. The emission signal integration time was 0.25 s. Milli-Q water was used as a reference. The EEMs were calibrated and normalized against the Raman scatter emission peak of the MilliQ water sample (Murphy et al., 2010), run on the same day and at the same excitation voltage as the corresponding samples. Raman normalization was performed using excitation at 350 nm and integrating the emission signal over the 380–426 nm spectral range, which reflects the closest measurable interval to the standard 381–426 nm range. CDOM absorption of the corresponding water samples was used for inner filter correction. The excitation and emission matrix spectra were processed using the drEEM toolbox implemented in the Matlab 2013R environment, according to the procedures described by Stedmon and Bro (2008) and Murphy et al. (2010, 2013). The PARAFAC model was applied to a data array of 984 × 53 × 176 (samples × excitation × emission). The results were validated by split-half validation (Harshman, 1984) applied to independent subsets (S4C6T3 – Splits, Combinations, Tests).

The PARAFAC model was run with a non-negativity constraint.

2.2.5 DOC concentrations measurements

The concentrations of Dissolved Organic Carbon (DOC) were measured in a HiPerTOC analyzer (Thermo Electron

Corp., Netherlands). The method used was based on UV/persulfate oxidation and NDIR (Non Dispersive Infra-Red) detection of evolving CO_2 (Sharp, 2002). To remove the residual dissolved CO_2, each of the acidified samples was purged with CO_2-free synthetic air. The precision of the measurement was determined from a triplicate analysis of each sample. Quality control consisted of the regular analysis of blanks, as well as accuracy checks based on comparisons with the reference material supplied by the Dennis Hansell Laboratory (University of Miami). The methodology ensured satisfactory accuracy (average recovery 93.1% of the certified CRM value; $n = 5$) and precision characterized by a relative standard deviation (RSD) of 2.5%.

2.2.6 Spectral indices

Based on measured DOM absorption and fluorescence spectra, the following spectral indices were calculated to describe DOM compositional properties:

(i) SUVA(254) – the carbon-specific absorption coefficient at 254 nm (Weishaar et al., 2003). This index was calculated following Equation (3):

$$\mathrm{SUVA}(254) = \frac{a_{\mathrm{CDOM}}(254)}{2.303 \times \mathrm{DOC}} \tag{3}$$

where: $a_{\mathrm{CDOM}}(254)$ is a CDOM absorption coefficient at 254 nm and DOC is a dissolved organic carbon concentration and the factor 2.303 is the natural logarithm of 10.

(ii) HIX – humification index, calculated according to Zsolnay et al. (1999) (Equation (4)) as the ratio of the emission spectrum (excited at 255 nm) integral over the spectral range 434–480 nm, $\sum_{480}^{434} I_{Em}$, to the integral of emission spectrum over the spectral range 300–345 nm (excited at the same wavelengths) $\sum_{345}^{300} I_{Em}$.

$$\mathrm{HIX} = \frac{H}{L} = \frac{\sum_{480}^{434} I_{Em}}{\sum_{345}^{300} I_{Em}} \tag{4}$$

(iii) I_p/I_h ratio calculated as the ratio of fluorescence intensity of identified protein-like components to the sum of fluorescence intensities of identified humic-like components:

$$I_p/I_h = \frac{I_{C4} + I_{C6}}{I_{C1} + I_{C2} + I_{C3} + I_{C5}} \tag{5}$$

where I_{Cn} represents the maximum fluorescence intensities (Fmax) of the respective component from C1 to C6 identified by the PARAFAC model at their respective excitation/emission maxima. I_{Cn} values reflect the relative contribution of each component to the total fluorescence signal, but do not represent integrated EEM fluorescence. The spectral characteristics and origins of these are given in Table S2.

2.3 Statistical analysis

Statistical analysis was performed using SigmaPlot 15.0 and STATISTICA 13.0. The normality of the data distribution was assessed using the Shapiro-Wilk test. As all of the data subsets deviated from a normal distribution, nonparametric tests were applied. The Mann-Whitney U test was used to evaluate differences between two groups (GCW, OW), while Kruskal-Wallis ANOVA on ranks followed by Dunn's post hoc test was used for multiple group comparison (SW, BSWW, BW). A p-value < 0.05 was considered statistically significant.

3. Results

Of the total 948 water samples collected during the study period, 498 were collected in the Gulf of Gdańsk, 350 in open waters, 84 in coastal waters, 24 in the Szczecin Lagoon, 18 in the Pomeranian Bay, and 10 in the Gulf of Finland. Taking into consideration a significantly smaller number of measurements, samples collected in the Szczecin Lagoon, Pomeranian Bay, and Gulf of Finland were used only while performing the PARAFAC analysis and then were excluded from further analysis. The final database was then divided into two subsets corresponding to the geographical boundaries of the Baltic Sea: Open Waters (OW) and Gulf and Coastal Water (GCW), which consisted of Gulf of Gdańsk merged together with coastal waters. Previous studies showed statistically significant differences in variability of selected inherent optical properties of seawater between these two regions (Sagan, 1991; Olszewski et al., 1992; Kowalczuk 1999; Kowalczuk et al., 1999, 2005a,b). Therefore, in this study, the two regions were analyzed separately to account for their contrasting optical characteristics. The geographical location of the sampling stations is presented in Figure 1. In the entire available data set, 70 stations with depths exceeding 60 meters were selected to analyze the variability of DOM fluorescence in the water column. At these stations (as shown in Figure 1), water samples were collected in vertical profiles. This data subset was categorized into subsets according to the location of the measurements: the Gulf of Gdańsk – Deep Waters (GGDW), and the Open Baltic – Deep Waters (OBDW). Based on existing knowledge about the optical properties of Baltic Sea water (Sagan, 1991; Olszewski et al., 1992; Sagan, 2008; Kratzer and Moore, 2018) and the hydrographic characteristics of the water masses, samples collected at various depths were classified into distinct water masses: SW – surface water (from 0 to 30 m depth), BSWW – Baltic Sea Winter Water (from 30 down to the depth of the permanent halocline, approximately 60 m depth), and BW – bottom waters located below the permanent halocline (Section 3.6).

To provide a better measure of the central tendency of the distribution and reduce sensitivity to extreme values, we mainly used the median and quantiles to describe the seasonal and annual variability of optical characteris-

Table 1. Minimum, maximum, median and 1st and 3rd quartiles of the physical properties of Baltic Sea water, chlorophyll *a* concentration and optical properties of CDOM; N – no. of samples.

	Salinity	Temperature [°C]	$a_{CDOM}(350)$ [m^{-1}]	$S_{300-600}$ [nm^{-1}]	Chl*a* [mg m^{-3}]	DOC [μmol L^{-1}]
	All data					
Min–Max	0.4–15.7	0.2–19.7	1.32–11.60	0.014–0.029	0.06–46.12	206–712
Median	7.2	9.9	1.85	0.022	3.1	349
Q_1, Q_3	7.0, 7.4	4.0, 14.6	1.68, 2.29	0.021, 0.023	1.54, 5.42	322, 380
N	741	741	859	859	804	762
	GCW					
Min–Max	0.4–12.2	0.2–19.7	1.32–11.60	0.017–0.026	0.10–46.12	220–712
Median	7.1	10.5	2.05	0.022	3.89	355
Q_1, Q_3	6.8, 7.4	3.9, 15.2	1.76, 2.55	0.021, 0.022	1.76, 2.55	326, 389
N	490	490	565	565	528	505
	OW					
Min–Max	6.4–5.7	0.2–18.3	1.33–4.73	0.014–0.029	0.06–12.66	206–471
Median	7.4	9.5	1.69	0.023	1.71	339
Q_1, Q_3	7.2, 7.6	4.3, 14.6	1.59, 1.82	0.022, 0.023	0.60, 3.13	313, 367
N	251	251	294	294	276	257

tics. However, mean values and standard deviations will also be reported to facilitate direct comparison with previous studies, as these metrics are commonly used in the CDOM/FDOM literature.

3.1 Hydrological conditions

The sampling was carried out between 2008 and 2013, from February to November, excluding the summer break period (June to August), when the r/v *Oceania* was unavailable for scientific research on the Baltic Sea.

During the research, the median water temperature was 10.0°C, with slightly higher values observed in GCW (10.7°C) compared to OW (9.5°C); however, the difference was not statistically significant. The median salinity measured for the entire data set was 7.2, with higher values observed in OW (7.4) than in GCW (7.1) (Table 1). This difference was statistically significant ($p < 0.05$), confirming distinct salinity regimes between the two regions. The lowest salinity value (0.4) was recorded at the ZN2 station (near the mouth of the Vistula River) in surface water (0 m). Salinity in water samples collected below the permanent halocline (below 40–80 m depth; Leppäranta and Myrberg, 2009) always exceeded 7.5.

3.2 DOC concentration

DOC concentration ranged from 206 μmol L^{-1} to 712 μmol L^{-1}, with lower values in open Baltic Sea waters and higher in GCW. The difference was statistically significant ($p < 0.05$). The median DOC concentration for the entire dataset was 349 μmol L^{-1} (Table 1). These values fell within typical Baltic Sea ranges and were elevated compared to oceanic values, reflecting terrestrial input and seasonal biological activity.

3.3 CDOM absorption

The spatial and seasonal distribution of CDOM in the southern Baltic followed well-established pattern described by Kowalczuk (1999) and Kowalczuk et al. (2005a,b, 2006). The median CDOM coefficient at 350 nm, $a_{CDOM}(350)$, in the analyzed dataset was 1.85 m^{-1} and was higher in GCW (1.97 m^{-1}) than in OW (1.69 m^{-1}) (Table 1). This difference was statistically significant ($p < 0.05$). The CDOM absorption slope coefficient, $S_{300-600}$, varied in a typical range found in marine waters (Stedmon and Nelson, 2015) from 0.014 nm^{-1} in March to 0.029 nm^{-1} in September, both obtained for OW samples (Table 1). The median values of $S_{300-600}$: 0.022 nm^{-1} in GCW, and 0.023 nm^{-1} in OW (Table 1), were significantly different ($p < 0.05$).

3.4 PARAFAC model and DOM fluorescence

Based on 984 measurements of dissolved organic matter fluorescence excitation/emission matrices, the PARAFAC model enabled the identification of six main groups of fluorophores (C1–C6) in Baltic Sea waters. Figure S3 presents the contour ploelden ring minimal route ts and the excitation/emission spectra loadings of the identified components, along with the split-half validation results. The excitation/emission characteristics of these identified components, along with their comparison to the peaks described by Coble (1996) and other authors are listed in the Table S2 (OpenFluor database; Murphy et al., 2014b).

The qualitative composition of FDOM in the Baltic Sea waters was predominantly comprised of terrestrial and marine humic-like substances (C1–C3,C5). Component C1 ($\lambda_{Ex}/\lambda_{Em}$ 250(300)/400 nm) was a mixture of humic-like substances of terrestrial (peak A – Coble, 1996) and marine origin (peak M – Coble, 1996). Component C2 ($\lambda_{Ex}/\lambda_{Em}$ 250(345)/418 nm) was a mixture of UV (peak A) and visible (peak C – Coble, 1996) humic-like substances. Com-

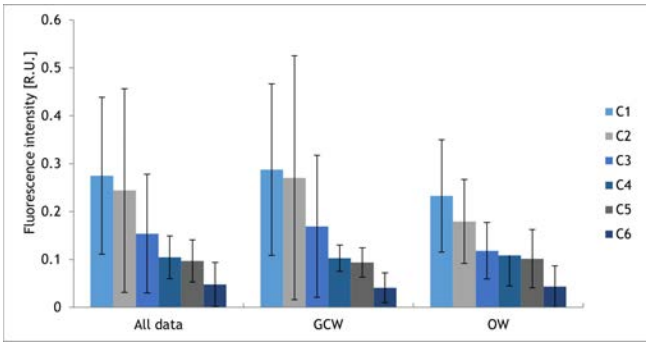

Figure 2. Composition of DOM fluorescence excitation/emission spectra in: whole data set (All data), Gulf of Gdańsk and Coastal Waters (GCW) and Open Waters (OW) of Baltic Sea in years 2008–2013. Bar plots represent average fluorescence intensity of 6 identified components, whiskers represents the standard deviation.

ponent C3 ($\lambda_{Ex}/\lambda_{Em}$ 260(375)/502 nm) was a mixture of UV humic-like substances (peak A) and soil fulvic acid (peak D – Stedmon et al., 2003).Component C5 ($\lambda_{Ex}/\lambda_{Em}$ 250/418 nm) was a typical example of humic-like fluorophores identified by Coble (1996) as peak A. Components C4 and C6 corresponded to amino acids derivatives in protein structures. Component C4 ($\lambda_{Ex}/\lambda_{Em}$ 285/348 nm) had spectral characteristics similar to Tryptophan, and Component C6 ($\lambda_{Ex}/\lambda_{Em}$ 270/292 nm) resembled spectral characteristics of Tyrosine.

The average composition of the FDOM components in the GCW and OW regions and in the combined data set ('All data') is presented in Figure 2. The average values of the fluorescence intensities of the identified DOM components were ranked for the whole data set as follows: $I_{C1} > I_{C2} > I_{C3} > I_{C4} > I_{C5} > I_{C6}$. The same compositional pattern was also found in two data subsets (GCW, OW). The statistical data relating to the fluorescence intensities of the PARAFAC components (I_{C1}–I_{C6}) and the total fluorescence intensity (I_{tot}) in the entire data set and in the distinguished regions are listed in Table 2. Higher average values of fluorescence intensity were observed in the GCW data set, and lower in the OW, for all components (C1–C6) and for I_{tot} and these differences were statistically significant ($p < 0.05$).

3.4.1 Spatial and seasonal variation of DOM fluorescence

The range of variability of the total FDOM – fluorescence intensity I_{tot}, in the Baltic Sea, was from 0.528 to 4.374 R.U., with the average value of $I_{tot} = 0.923$ R.U., and the median value of $I_{tot} = 0.719$ R.U. (Table 2). However, the range of variability in total FDOM fluorescence intensity differed between the studied regions. In the GCW, the range of variability of the I_{tot} was: $0.549 \geq I_{tot}$ (GCW) ≤ 4.374 R.U. and almost overlapped with the range of variability determined for all data. The average value of the total fluorescence intensity in the GCW was: $I_{tot} = 0.996$ R.U., with the median of $I_{tot} = 0.777$ R.U. Such a wide range of I_{tot} variation in coastal and bay waters, expressed by a very high value of the standard deviation (0.615 R.U.) and a high value of the coefficient of variation (61.05%) is typical for water bodies experiencing cyclical hydro-meteorological phenomena. In the Baltic Sea, these fluctuations are associated with the riverine hydrological cycle, particularly in the Gulf of Gdańsk and the coastal zone, where freshwater inflows and wind-driven dynamic contribute to intensive mixing of riverine with marine waters.

In contrast, the range of variability of the I_{tot} in the OW within: $0.528 \geq I_{tot(OW)} \leq 2.420$ R.U., and was much narrower compared to one found in the GCW. The observed maximum $I_{tot(OW)}$ value was 2.420 R.U., almost half of those in the GCW. In the OW, the minimum $I_{tot(OW)}$ value (0.528

Table 2. Minimum, maximum, median and 1st and 3rd quartiles of fluorescence intensities of six identified components and the total fluorescence intensity in whole data set and in Gulf and Coastal Waters (GG),) and Open Waters (OW) of Baltic Sea; N – number of samples.

	I_{C1} [R.U.]	I_{C2} [R.U.]	I_{C3} [R.U.]	I_{C4} [R.U.]	I_{C5} [R.U.]	I_{C6} [R.U.]	I_{tot} [R.U.]
				All data			
Min–Max	0.155–1.263	0.115–1.765	0.080–1.017	0.031–0.380	0.027–0.400	0.000–0.415	0.528–4.374
Median	0.215	0.172	0.11	0.095	0.089	0.034	0.719
Q_1, Q_3	0.199, 0.262	0.152, 0.128	0.099, 0.142	0.086, 0.107	0.083, 0.097	0.022, 0.052	0.657, 0.880
N	860	860	860	860	860	860	860
				GCW			
Min–Max	0.166 –1.263	0.116–1.765	0.080–1.017	0.031–0.341	0.027–0.400	0.000–0.415	0.549–4.374
Median	0.229	1.184	0.118	0.097	0.09	0.035	0.777
Q_1, Q_3	0.206, 0.286	0.161, 0.263	0.104, 0.163	0.088, 0.110	0.083, 0.099	0.023, 0.054	0.686, 0.968
N	565	565	565	565	565	565	565
				OW			
Min–Max	0.155–0.818	0.115–0.570	0.080–0.359	0.062–0.380	0.034–0.354	0.000–0.318	0.528–2.420
Median	0.2	0.156	0.101	0.09	0.089	0.03	0.666
Q_1, Q_3	0.185, 0.212	0.138, 0.172	0.092, 0.110	0.083, 0.102	0.082, 0.095	0.020, 0.049	0.620, 0.707
N	295	295	295	295	295	295	295

R.U.) was also the lowest one observed in the entire data set. The average and median values of the $I_{\mathrm{tot(OW)}}$ were much lower, $I_{\mathrm{tot(OW)}} = 0.7849$ R.U. and $I_{\mathrm{tot(OW)}} = 0.666$ R.U., respectively. The total fluorescence intensity of DOM in open Baltic waters also exhibits lower variability compared to GCW with a standard deviation of 0.41 R.U.

The highest average fluorescence intensity of component C1, corresponding to humic substances of terrestrial and marine origin, was observed in the GCW and amounted to 0.288 ± 0.179 R.U., while in the open waters of the Baltic Sea to 0.232 ± 0.117 R.U. A similar spatial distribution of mean fluorescence intensities was observed for component C2, representing terrestrial and marine humic-like substances, and component C3, corresponding to terrestrial humic-like substances (values given in Table 2). In contrast, the spatial distribution of the mean fluorescence intensities for component C4, associated with protein-like substances similar to tryptophan, and component C6, related to protein-like substances similar to tyrosine, and humic-like component C5, was characterized by higher values in OW and lower values in GCW. The mean fluorescence intensities of components C4, C5, and C6 in OW were: C4 – 0.109 ± 0.064 R.U., C5 – 0.102 ± 0.061 R.U., C6 – 0.044 ± 0.043 R.U., compared to those found in the GCW: C4 – 0.103 ± 0.028 R.U., C5 – 0.094 ± 0.031 R.U., C6 – 0.041 ± 0.031 R.U, respectively.

The seasonal variability of total DOM fluorescence in the GCW in the Baltic Sea ($I_{\mathrm{tot(GCW)}}$) was characterized by a distinct pattern with a period of higher values (Figure 3) that occurred in spring: March to April. The median $I_{\mathrm{tot(GCW)}}$ value in February was 0.719 R.U., followed by a slight increase in March (0.852 R.U.), and its maximum in April (0.884 R.U.). In May, there was a change in the median $I_{\mathrm{tot(GCW)}}$ to 0.810 R.U. The absence of measurements in June and July makes it difficult to determine when the first part of the cycle ends. In September, the median $I_{\mathrm{tot(GCW)}}$ decreased further (0.735 R.U.), reaching its minimum in October ($I_{\mathrm{tot(GCW)}} = 0.706$ R.U.). In November, there was observed slight increase in the median total DOM fluorescence in GCW ($I_{\mathrm{tot(GCW)}} = 0.762$ R.U.). The differences between the first and second part of a year were statistically significant.

The annual cycle of the first three components (C1 to C3) (Figure S4) in GCW corresponded to the annual cycle of the total DOM fluorescence in GCW. Fluorescence intensities of each of these components were characterized by an increase in median values from the beginning of the year to April, followed by a sharp decline in May. In October, there was a slight increase in median fluorescence intensity of components C2 and C3. The median value of the component C1 fluorescence intensity remained similar in September and October. In November, a minimum was observed in the median values of the fluorescence intensities of components C1 to C3. The differences were statistically significant between the first and second part of a year. The annual cycle of variability of the fluorescence intensity of component C5, corresponding to terrestrial humic-like substances, differed from the fluorescence intensity variability of components C1 to C3 (Figure S4). It showed a steady increase in the median value of I_{C5} from February until May. In September, then there was a noticeable drop of I_{C5} median value to a similar level as observed in March (no statistically significant differences). Similarly to components C2 and C3, there was a slight increase in the median fluorescence intensity of component C5 in October, followed by another decrease in November to the lowest level in the year (Figure S4). The annual cycle of the humic-like components in the bay and coastal waters of the Baltic Sea ($I_{h(\mathrm{GCW})} = I_{\mathrm{C1(GCW)}} + I_{\mathrm{C2(GCW)}} + I_{\mathrm{C3(GCW)}} + I_{\mathrm{C5(GCW)}}$) (Figure 3) exhibited higher values from March to May, with the maximum in March (1.005 R.U.). In the second half of a year, $I_{h(\mathrm{GCW})}$ declined significantly. The minimum $I_{h(\mathrm{GCW})}$ value was observed in February (0.577 R.U.). The annual cycles of fluorescence intensity of the protein-like components C4 and C6 were significantly different from each other (Figure S4). The annual variation in the median fluorescence intensity for component C4 featured a maximum in the median fluorescence intensity in April. From September there was a gradual decrease in the median fluorescence intensity of component C4, reaching its minimum in November. The variability of the median fluorescence intensity of the protein-like component C6, over the course of the year, was different from the variability of the other components. The local maximum in the median fluorescence intensity of component C6 was observed in March. In April, there was a decrease, and a minimum was observed in May (0.028 R.U.). In September, there was another local maximum, and in October, it reached its minimum in the annual cycle (0.027 R.U.), and then it was subsequently increasing in November. The annual cycle of the protein-like components in GCW of the Baltic Sea ($I_{p(\mathrm{GCW})} = I_{\mathrm{C4(GCW)}} + I_{\mathrm{C6(GCW)}}$ (Figure 3) was characterized by a maximum median fluorescence intensity in March (0.176 R.U.), followed by lower values during the next months, until it increased again in September (0.164 R.U.) and dropped again to the minimum in October (0.125 R.U.). In November there was an increase of $I_{p(\mathrm{GCW})}$, to the a value of 0.153 R.U.

The seasonal variability of the total DOM fluorescence in the open waters of the Baltic Sea ($I_{\mathrm{tot(OW)}}$) is shown in Figure 3. Changes in the fluorescence intensity variability over the course of a year in OW were minor. The highest median of $I_{\mathrm{tot(OW)}}$ was observed in March (0.682 R.U.) and the lowest in October (0.650 R.U.). The median values of total fluorescence intensity in other months were as follows: April – 0.677 R.U., May – 0.670 R.U., September – 0.650 R.U. Only the differences between March and September and March and October were statistically significant. The median of fluorescence intensity of compo-

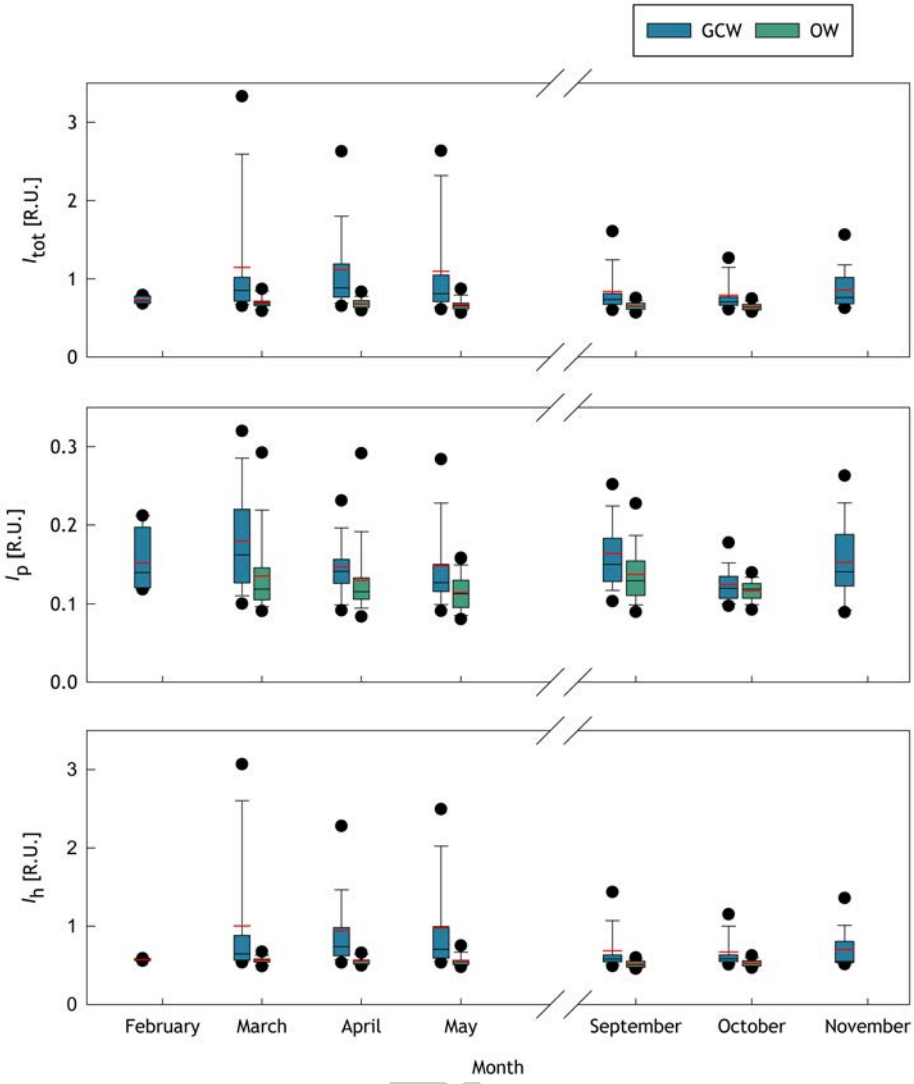

Figure 3. Monthly aggregated total dissolved organic matter fluorescence intensity (I_{tot}), fluorescence intensity of protein-like components (I_p), and fluorescence intensity of humic-like components (I_h) over six years in GCW and OW of the Baltic Sea. Median values are marked with the red solid line, mean values are marked with the black solid line, 10th and 90th percentiles are marked with the whiskers, and25 th and 75th percentiles with the box. Dots represents outliers. Note different y-axes scales.

nent C1 in OW decreased slightly from March (0.207 R.U.) to September (0.189 R.U.) (Figure S4). Similarly, the median fluorescence intensity of component C2 was also highest in March (0.162 R.U.). On the other hand, the respective median values of fluorescence intensity of component C3 and C5 reached their maxima in May ($I_{\mathrm{C3(OW)}} = 0.105$ R.U., $I_{\mathrm{C5(OW)}} = 0.094$ R.U.). Conversely, in September, the respective median values of fluorescence intensity of all humic-like components (C1–C3, C5) were at their minimum ($I_{\mathrm{C1(OW)}} = 0.189$ R.U., $I_{\mathrm{C2(OW)}} = 0.139$ R.U., $I_{\mathrm{C3(OW)}} = 0.095$ R.U., $I_{\mathrm{C5(OW)}} = 0.086$ R.U.) (Figure S4). The annual cycle of the humic-like components in the open waters of the Baltic Sea ($I_{h(\mathrm{OW})} = I_{\mathrm{C1(OW)}} + I_{\mathrm{C2(OW)}} + I_{\mathrm{C3(OW)}} + I_{\mathrm{C5(OW)}}$) (Figure 3) exhibited monthly fluctuations with the highest value in March (0.564 R.U.), and the lowest in September (0.517 R.U.). The differences between the first and second part of a year were statistically significant ($p < 0.05$). Component C4 exhibited the highest median value of the fluorescence intensity in May (0.091 R.U.), and the lowest in October (0.086 R.U.). Furthermore, the median value of the component C6 fluorescence intensity reached maximum in September (0.040 R.U.) and two minima in March and October (0.028 R.U.) (Figure S4). The annual cycle of the protein-like components in the open waters of the Baltic Sea ($I_{p(\mathrm{OW})} = I_{\mathrm{C4(OW)}} + I_{\mathrm{C6(OW)}}$ (Figure 3) was characterized by two maxima, in September (0.137 R.U.) and in March (0.135 R.U.) and a minimum in May (0.114 R.U.). Differences between the medians of all six components

were statistically significant between the first and second part of a year.

3.5 Spatial and annual distribution of the HIX index, I_p/I_h ratio, and a carbon specific absorption coefficient, SUVA(254)

The range of variability in the HIX values determined for the entire data set contained within 2.154 and 17.688, with a median of 4.074 (Table 3). In GCW, the values of $HIX_{(GCW)}$ were between 2.339 and 17.668, nearly identical to the range determined for all data. The $HIX_{(GCW)}$ median value was 4.271. In contrast, the range of variability in $HIX_{(OW)}$ values was significantly smaller, and contained from 2.154 to 5.885. The $HIX_{(OW)}$ median value was 3.803.

The annual variability in the $HIX_{(GCW)}$ values in GCW showed two periods of elevated values (Figure 4). The first increase in median $HIX_{(GCW)}$ values was observed in March (4.275) and reached a maximum in April (4.821). In May, there was a decrease in the median $HIX_{(GCW)}$ to 4.583. The annual $HIX_{(GCW)}$ minima were noted in February (3.634) and in September (3.718). The low HIX value indicated a lower saturation of DOM with polyaromatic compounds. The annual cycle of the median $HIX_{(OW)}$ values showed a pattern similar to that observed in GCW – the highest $HIX_{(OW)}$ value was recorded in April (4.116) and the lowest in September (3.456).

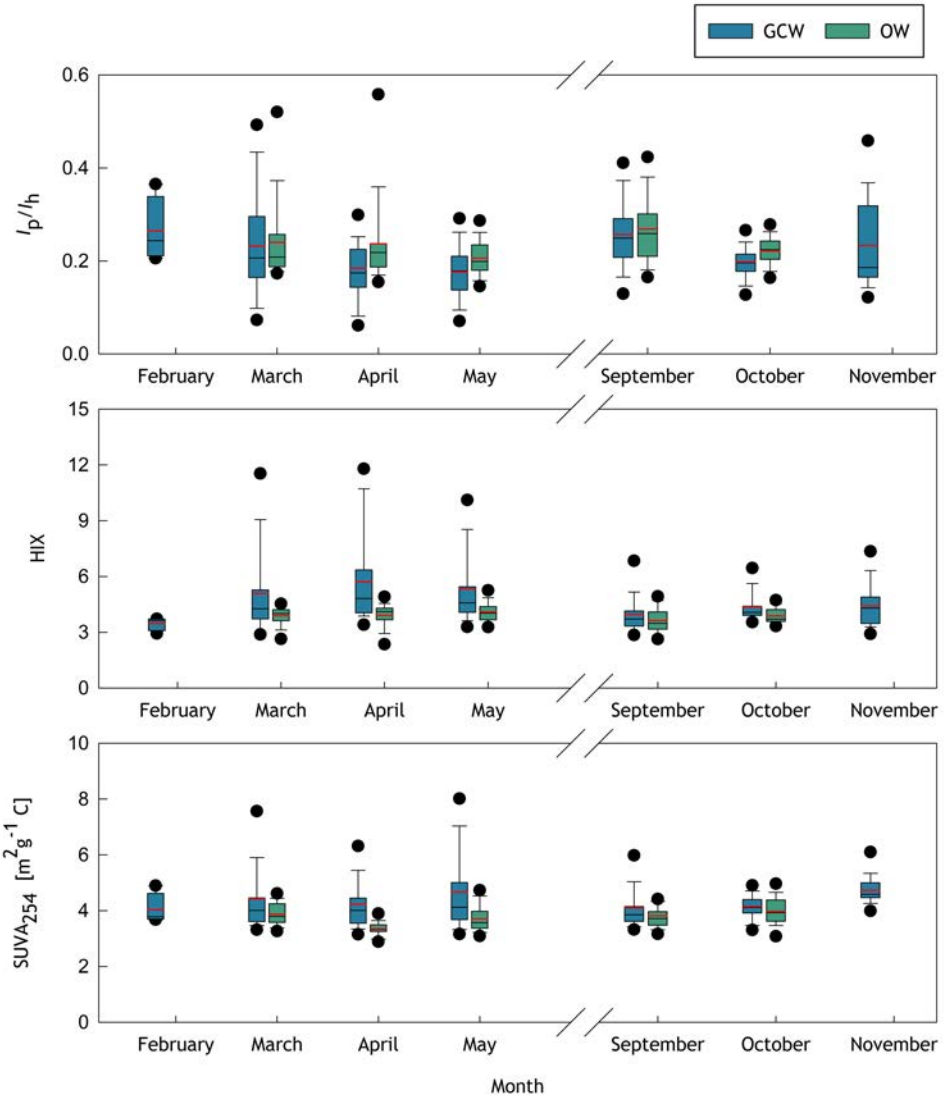

Figure 4. Monthly aggregated dissolved organic matter fluorescence intensity of protein-like to humic-like components ratio (I_p/I_h), Humification Index (HIX) and carbon specific absorption coefficient (SUVA(254)) over six years in GCW and OW of the Baltic Sea. Median values are marked with the red solid line, mean values are marked with the black solid line, 10th and 90th percentiles are marked with the whiskers, and 25th and 75th percentiles with the box. Dots represents outliers. Note different y-axes scales.

Table 3. Minimum, maximum, median and 1st and 3rd quartiles of fluorescence intensities of carbon specific absorption coefficient (SUVA(254)), Humification Index (HIX) and dissolved organic matter fluorescence intensity of protein-like to humic-like components ratio (I_p/I_h), in whole data set and in Gulf and Coastal Waters (GG), and Open Waters (OW) of Baltic Sea; N – number of samples.

	SUVA(254) [m^2 gC^{-1}]	HIX	I_p/I_h
	All data		
Min–Max	1.027–5.828	2.154–17.688	0.038–0.631
Median	1.701	4.074	0.213
Q_1, Q_3	1.548, 1.898	3.612, 4.664	0.178, 0.267
N	761	859	860
	GCW		
Min–Max	1.027–5.828	2.339–17.688	0.038–0.637
Median	1.757	4.226	0.202
Q_1, Q_3	1.596, 1.967	3.754, 5.054	0.165, 0.245
N	504	564	565
	OW		
Min–Max	1.160–4.047	2.154–5.885	0.130–0.641
Median	1.592	3.799	0.225
Q_1, Q_3	1.488, 1.746	3.434, 4.222	0.192, 0.264
N	257	295	295

Based on the conclusion of the study by Kowalczuk et al. (2013), the ratio of the sum of the fluorescence intensity of protein-like FDOM components to the sum of the fluorescence intensities of humic-like FDOM components, I_p/I_h, was used as an indicator of the presence of autogenic DOM. The range of I_p/I_h values determined for the entire data set was 0.038 to 0.641, with a median value of 0.213. The variability of I_p/I_h values differed significantly across the studied regions ($p < 0.05$). In GCW, the range of $I_p/I_{h(GCW)}$ was from 0.038 to 0.637 with a median of 0.202. The range of $I_p/I_{h(OW)}$ in OW was greater than in GCW, and it was shifted toward higher values (from 0.130 to 0.640). The median $I_p/I_{h(OW)}$ value was 0.225.

The annual cycle of $I_p/I_{h(GCW)}$ values in GCW exhibited an opposite cycle compared to the annual cycle of $HIX_{(GCW)}$ (Figure 4). The median $I_p/I_{h(GCW)}$ value in February was 0.244. In March, the median value decreased to 0.207, reaching the annual minimum in April (0.174). In May, the median $I_p/I_{h(GCW)}$ increased slightly in May to a value of 0.178. The median $I_p/I_{h(GCW)}$ value reached its annual maximum in September (0.249). The median $I_p/I_{h(GCW)}$, declined to 0.196 in October and to 0.186 in November (no statistically significant difference between those two).

The annual cycle of $I_p/I_{h(OW)}$ observed in the open waters of the Baltic Sea, was similar to observed in GCW. In March, there was the lowest median value of $I_p/I_{h(OW)}$ – 0.208. Elevated $I_p/I_{h(OW)}$ median values were also observed in following spring months, in April (0.218) and May (0.215), showing no statistically significant deviation from the March median (Figure 4). In September, the median $I_p/I_{h(OW)}$ value reached its maximum (0.259).

The SUVA(254) index is correlated with the number of aromatic rings in DOM molecules (Weishaar et al., 2003). The observed range of SUVA(254) values in the Baltic Sea was between 1.027 and 5.828 m^2 gC^{-1}, with a median of 1.701 m^2 gC^{-1} (Table 3). In the GCW, the range of $SUVA(254)_{(GCW)}$ variability overlapped with one reported for the entire data set. The median $SUVA(254)_{(GCW)}$ was 1.757 m^2 gC^{-1}. The range of variability of $SUVA(254)_{(OW)}$ values in OW was smaller, between 1.160 and 4.047 m^2 gC^{-1}. The median $SUVA(254)_{(OW)}$ was 1.592 m^2 gC^{-1}. The annual cycle variability of the median $SUVA(254)_{(GCW)}$ values was characterized by stability in the winter and spring months (Figure 4, Table 3). The median $SUVA(254)_{(GCW)}$ values in March (1.740 m^2 gC^{-1}, April (1.739 m^2 gC^{-1}) and May (1.788 m^2 gC^{-1}) did not show a statistically significant difference ($p > 0.05$). This situation indicated a very strong influence of terrestrial DOM on the FDOM composition. In September, a statistically significant ($p < 0.05$) decrease in median $SUVA(254)_{(GCW)}$ value to 1.673 m^2 gC^{-1} was observed, followed by a subsequent increase in October (1.786 m^2 gC^{-1}). The median $SUVA(254)_{(GCW)}$ reached its maximum value in November (1.990 m^2 gC^{-1}).

In the open Baltic Sea, the $SUVA(254)_{(OW)}$ underwent dynamic fluctuations throughout the year. The most significant changes were observed in the first half of the year. There was a relatively high median $SUVA(254)_{(OW)}$ observed in March (1.647 m^2 $g\,C^{-1}$), and there was a decrease in April (1.857 ^{2} $g\,C^{-1}$) followed by an increase in May (1.444 ^{2} $g\,C^{-1}$) and September (1.612 ^{2} $g\,C^{-1}$), reaching the annual maximum in October (1.703 ^{2} $g\,C^{-1}$). All differences were statistically significant ($p < 0.05$).

3.6 Environmental variables controlling the variability of FDOM

The DOM fluorescence intensity depends on the amount of energy absorbed by CDOM. The existence of a linear relationship between the light absorption coefficient of CDOM ($a_{CDOM}(\lambda)$) and the total fluorescence intensity of DOM (I_{tot}) has been well documented (Ferrari and Tassan, 1991; Ferrari and Dowell, 1998; Kowalczuk et al., 2005a,b, 2010). The regression analysis between $a_{CDOM}(350)$ and I_{tot} calculated for our data set, confirmed a close, linear relationship between those parameters with a very high correlation coefficient, R = 0.97 (Figure 5). Such a close linear relationship between $a_{CDOM}(350)$ and I_{tot} allowed the use of DOM fluorescence measurements as a proxy of CDOM absorption level in the Baltic Sea. Further analysis revealed that the strong relationship between $a_{CDOM}(350)$ and I_{tot} results from the presence of "humic-like" fraction in FDOM mixture (Figure 5).

Regression analysis between the total fluorescence intensity of DOM and salinity revealed a significant correlation ($R = -0.90$), particularly in the mixed layer from

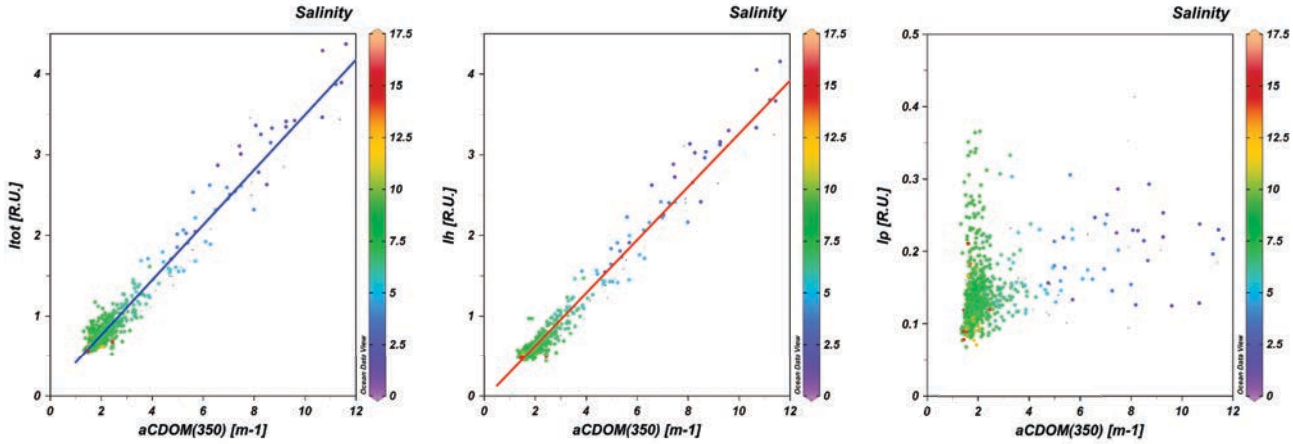

Figure 5. Distribution of total dissolved organic matter fluorescence intensity (I_{tot}), fluorescence intensity of humic-like components (I_h), and fluorescence intensity of protein-like components (I_p) in relation to light absorption by CDOM ($a_{\mathrm{CDOM}}(350)$). Color bar shows sampled depth.

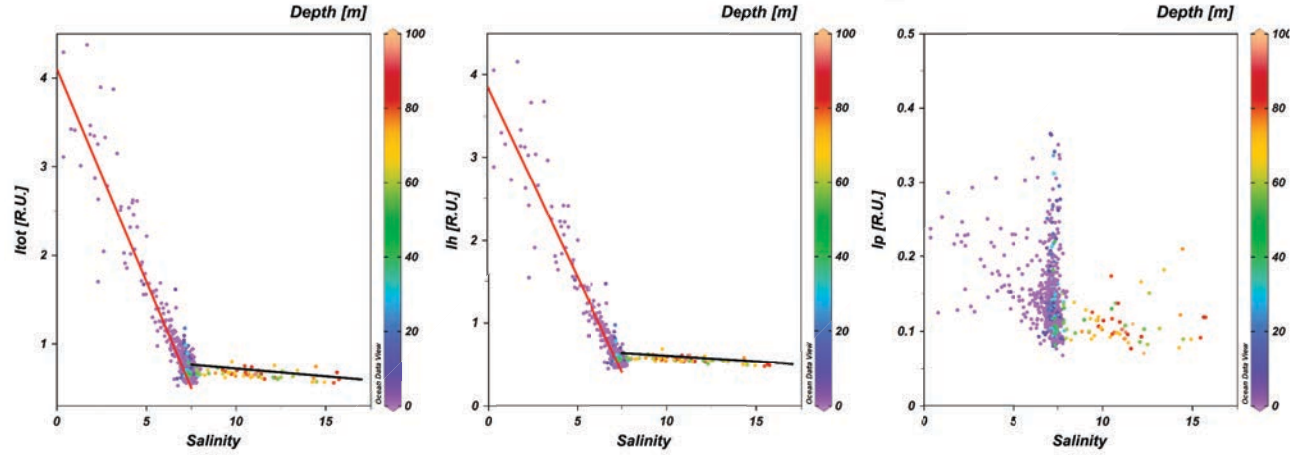

Figure 6. Distribution of total dissolved organic matter fluorescence intensity (I_{tot}), fluorescence intensity of humic-like components (I_h), and fluorescence intensity of protein-like components (I_p) in relation to salinity. Color bar shows sampled depth.

the surface to 30 m deep, with salinity below 7.5. This indicates that the mixing of freshwater with marine water is a key factor influencing the distribution of FDOM in the southern Baltic Sea. An even stronger inverse correlation with salinity showed the humic-like fraction of DOM (I_h) ($R = -0.91$) (Figure 6). In water samples collected from areas where salinity is 7.5 or higher, and at depths greater than 30 m, there was only a slight decrease in both, total ($R = -0.32$) and humic-like ($R = -0.56$) DOM fluorescence intensity with increasing salinity (Figure 6). Analysis of the relationship between fluorescence intensity of protein-like components and salinity (Figure 6), together with results from previous studies (Kowalczuk et al., 2015; Reader et al., 2019; Terzić et al., 2024; Loginova et al., 2024), suggests that protein-like components in the Baltic Sea originate primarily from autochthonous sources such as phytoplankton blooms and microbial activity. Unlike humic-like fluorescence, I_p did not show a clear relationship with salinity below 7.0, indicating that its distribution was mainly driven by local biological production rather than the mixing process. At higher salinity (>7.5), microbial transformation of DOM and sediment-related inputs may also contribute to the observed variability. The correlation between fluorescence intensity of component C4, I_{C4}, and chlorophyll *a* concentration (Figure 7, Table 4), described by a power function, although weak ($R = 0.45$), indicated that component C4 was formed locally through phytoplankton activity or degradation. Similarly, Terzić et al. (2024) reported a comparable yet stronger relationship ($R = 0.77$) between $a_{\mathrm{LH}}(676)$ (an optical proxy to estimate chlorophyll *a* concentration; Roesler and Barnard, 2013) and FDOM-Ch3 (the fluorescence intensity of the protein-like fraction of FDOM) in surface waters of the Baltic Sea. The negative correlation ($R = -0.84$) between the Humification Index (HIX) and salinity found in the mixed layer (salinity below 7.5) of the Baltic Sea (Figure 8)

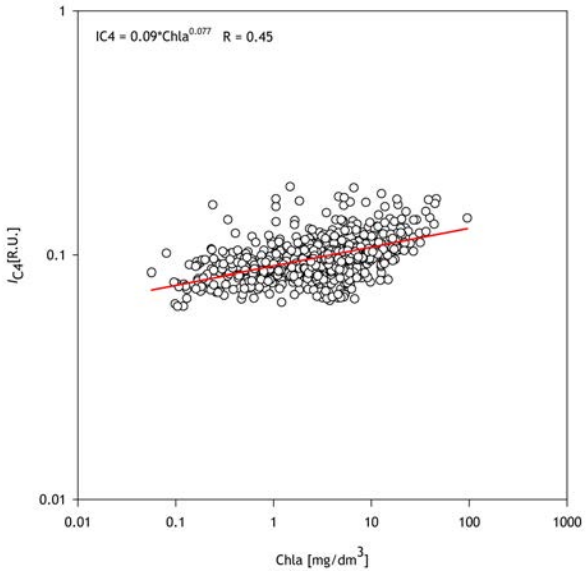

Figure 7. Distribution of the fluorescence intensity of the protein-like component C4, IC4, in relation to chlorophyll *a* concentration (Chl*a*).

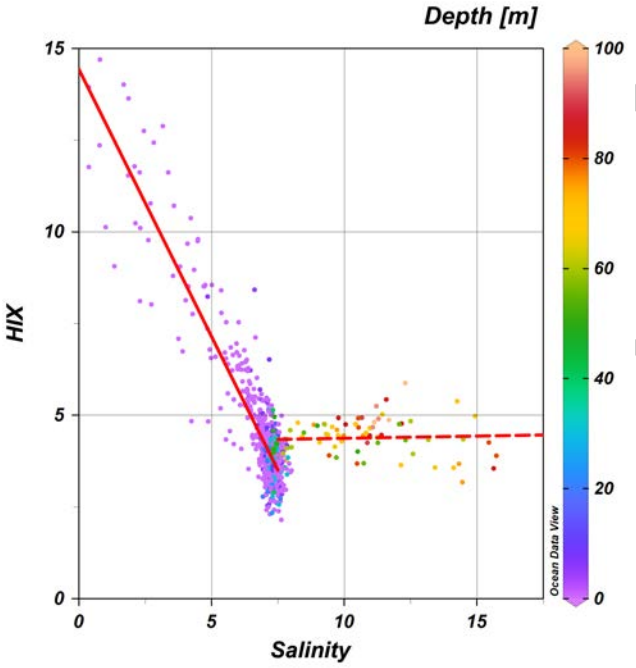

Figure 8. Distribution of the Humification Index (HIX) in relation to salinity. Color bar shows sampled depth.

was an evidence that DOM delivered to its environment had typically a high molecular weight and was enriched in aromatic structures – characteristics that are associated with higher HIX values (Zsolney et al., 1999; Huguet et al., 2009) – which decrease during water masses mixing. In the water below pycnocline, HIX values remained relatively stable and showed no clear correlation with salinity ($R = 0.011$) (Figure 8) suggesting that the humification process in deeper layers was less influenced by salinity gradients. Minor fluctuations in HIX may result from the input of organic matter from sediments or its microbial transformation, enriching FDOM with humic-like components (Kowalczuk et al., 2015; Loginova et al., 2024).

3.7 Vertical variability of DOM fluorescence in the Gulf of Gdańsk and the Open Baltic waters

To characterize hydrographic and optical conditions on the vertical scale, the distributions of median values of salinity, temperature, $a_{\mathrm{CDOM}}(350)$, and $S_{300-600}$, in distinct water masses occurring in the Gulf of Gdańsk and the open Baltic Sea deep stations (GGDW and OBDW, respectively) are presented in Figure 9 and Figure 10.

The lowest salinity (6.4) in the data set was recorded in the surface water (SW) of the Gulf of Gdańsk (GGDW), attributed to the mixing of freshwater of the Vistula River with seawater. In GGDW, salinity values increased with depth, reaching a median of 10.4 in the Bottom Water (BW). The respective water masses in the OBDW data subset were more saline. The salinity median values were: $S = 7.3$ in the SW, $S = 7.4$ in the Baltic Sea Winter Water (BSWW), and $S = 10.8$ in the BW, due to longer distance from freshwater source and easier penetration of more saline water from the Danish Straits (Figure 9). The differences in salinity across depth layers were statistically significant in both regions.

The median values of the temperature (Figure 9) reflected the intensity of thermodynamic processes at the Baltic Sea surface. The highest median temperature and the broadest range of temperature fluctuations were observed in the surface layer in both GGDW (T = 10.9°C) and OBDW (T = 11.0°C) stations. This variation was linked to the seasonal heating of the sea surface layer due to the absorption of solar radiation, and its cooling due to the emission of long-wave thermal radiation. The BSWW, which is controlled by the convective mixing of surface water with deeper layers during winter, exhibited the smallest range of variability in temperature. The median temperature in BSWW was 3.1°C in GGDW, and 3.5°C in OBDW. In the deep waters of the southern Baltic Proper (OBDW), the median temperature (T = 5.2°C) was approximately 1.0°C higher than in the GGDW. In both areas, temperature differences between layers were statistically significant.

The vertical distribution of $a_{\mathrm{CDOM}}(350)$ exhibits distinct patterns in GGDW and OBDW (Figure 10). In the GGDW, the highest values of $a_{\mathrm{CDOM}}(350)$, were observed in surface waters (1.81 m^{-1}), decreasing in the Baltic Sea Winter Water ($a_{\mathrm{CDOM}}(350) = 1.65\ \mathrm{m}^{-1}$) and the Bottom Water ($a_{\mathrm{CDOM}}(350) = 1.65\ \mathrm{m}^{-1}$). In OBDW, the median value of $a_{\mathrm{CDOM}}(350)$ in the Bottom Water was 1.65 m^{-1}, followed by a slight increase in the BSWW ($a_{\mathrm{CDOM}}(350) = 1.68\ \mathrm{m}^{-1}$) and then a small decrease in the SW (a_{CDOM}

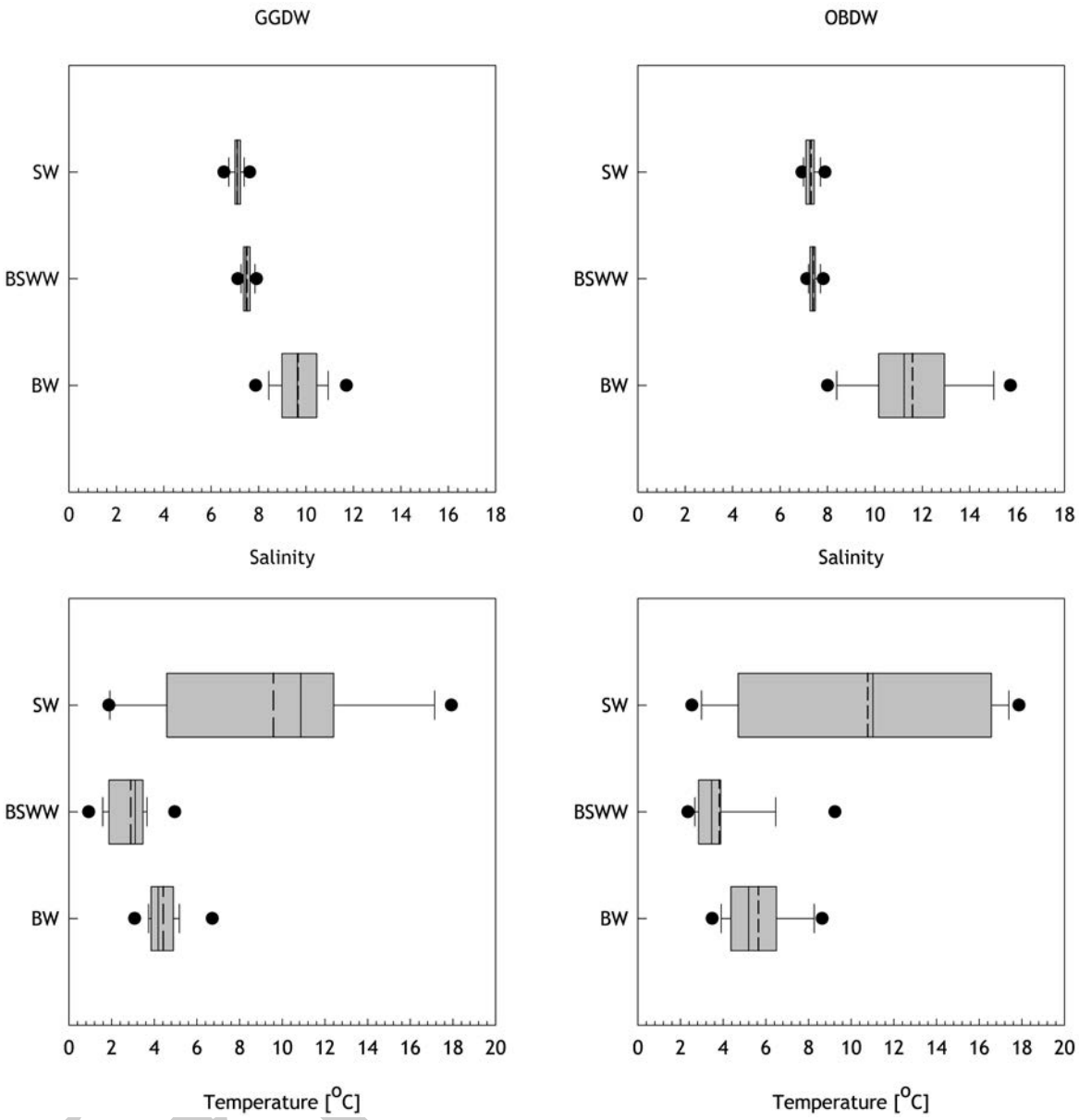

Figure 9. Median distribution of salinity and temperature in different water layers in the Gulf of Gdańsk Deep Waters (GGDW) and the Open Baltic Deep Waters (OBDW). Median values are marked with the solid line, mean values are marked with the dashed line, 10th and 90th percentiles are marked with the whiskers, and 25th and 75th percentiles with the box. SW – Surface Water, BSWW – Baltic Sea Winter Water, BW – Bottom Water.

(350) = 1.63 m^{-1}). However, in this region, the differences between layers were statistically insignificant. The vertical distributions of $S_{300-600}$ in both GGDW and OBDW exhibited the opposite vertical distribution compared to $a_{CDOM}(350)$ (Figure 10), having the lowest median values in BW, and the highest in BSWW (GCWD) and in SW (OBWD). Significant differences were found between SW and BW in both areas, and between SW and BSWW in OBDW.

The box plots presented in Figure 11 show the average fluorescence intensities, and standard deviations, of the identified components in various hydrographic water masses. The graph revealed a notable degree of similarity, indicating a relatively consistent composition of FDOM throughout the examined areas of the Baltic Sea. In this composition, humic-like components are predominant. In contrast, protein-like components contributed less to the total fluorescence intensity. The arrangement of these components remains uniform across the selected regions and the various vertical layers of water, with only slight variations in the values of individual components within specific regions and water masses.

Table 4. Regression analysis of the selected parameters.

Dependent	Independent	Condition(s)	Equation	R	N
I_{tot}	$a_{\mathrm{CDOM}}(350)$	–	$I_{\mathrm{tot}} = 0.342 \times a_{\mathrm{CDOM}}(350) + 0.078$	0.97	822
I_h	$a_{\mathrm{CDOM}}(350)$	–	$I_h = 0.330 \times a_{\mathrm{CDOM}}(350) - 0.036$	0.98	822
I_{tot}	Salinity	Salinity ≤ 7.5 Depth ≤ 30 m	$I_{\mathrm{tot}} = -0.471 \times \mathrm{Salinity} + 4.102$	−0.95	598
I_{tot}	Salinity	Salinity > 7.5 Depth > 30 m	$I_{\mathrm{tot}} = -0.010 \times \mathrm{Salinity} + 0.768$	−0.44	70
I_h	Salinity	Salinity ≤ 7.5 Depth ≤ 30 m	$I_h = -0.455 \times \mathrm{Salinity} + 3.847$	−0.95	602
I_h	Salinity	Salinity > 7.5 Depth > 30 m	$I_{\mathrm{tot}} = -0.002 \times \mathrm{Salinity} + 0.565$	−0.13	124
HIX	Salinity	Salinity ≤ 7.5	$\mathrm{HIX} = -1.460 \times \mathrm{Salinity} - 0.904$	−0.90	626
HIX	Salinity	Salinity > 7.5	$\mathrm{HIX} = 0.030 \times \mathrm{Salinity} + 4.028$	0.12	76
$S_{300-600}$	HIX	–	$S_{300-600} = 0.011 \times \exp(-0.107 \times \mathrm{HIX}) + 0.015$	0.71	845
I_{C4}	Chl$a$	–	$I_{\mathrm{C4}} = 0.09 \times \mathrm{Chl}a^{0.077}$	0.44	771

Figure 12 presents the vertical distribution of median values of fluorescence intensities of the first three components: C1, C2, and C3, in the GGDW and the open Baltic Sea (OBDW). There were noticeable differences between these two regions: in the GGDW, the median values of fluorescence intensities of the humic-like components were higher compared to the OBDW. In the gulf and coastal waters of the Baltic Sea, a slight decrease in the median of fluorescence intensities values of components C1 through C3, was observed in the BSWW ($I_{\mathrm{C1(GGDW)}} = 0.204$ R.U., $I_{\mathrm{C2(GGDW)}} = 0.160$ R.U., $I_{\mathrm{C3(GGDW)}} = 0.105$ R.U.), followed by a statistically significant (Kruscal-Wallis test, $p < 0.01$) increase in these values in BW for components C2 ($I_{\mathrm{C2(GGDW)}} = 0.179$ R.U.), component C1 ($I_{\mathrm{C1(GGDW)}} = 0.206$ R.U.) and component C3 ($I_{\mathrm{C3(GGDW)}} = 0.112$ R.U.). However, it should be noted that for components C1 and C3, the differences between the water layers were not statistically significant, while for C2, a significant variation was observed only between the BW and BSWW layers. A different pattern was observed in the vertical distribution of the median fluorescence intensity values for components C1, C2, and C3 in the open waters of the Baltic Sea. In this region, the lowest median values of the fluorescence intensity for these components was observed in the surface layer, ($I_{\mathrm{C1(OBDW)}} = 0.188$ R.U., $I_{\mathrm{C2(OBDW)}} = 0.139$ R.U., $I_{\mathrm{C3(OBDW)}} = 0.095$ R.U.), with an increase in the BSWW ($I_{\mathrm{C1(OBDW)}} = 0.206$ R.U., $I_{\mathrm{C2(OBDW)}} = 0.155$ R.U., $I_{\mathrm{C3(OBDW)}} = 0.101$ R.U.), and the highest values in BW ($I_{\mathrm{C1(OBDW)}} = 0.204$ R.U., $I_{\mathrm{C2(OBDW)}} = 0.176$ R.U., $I_{\mathrm{C3(OBDW)}} = 0.109$ R.U.). The difference in I_{C1} between BSWW and BW layers was not statistically significant, and similarly, no significant differences were observed for components C2 and C3 between SW and BSWW. The vertical distribution of median values of the fluorescence intensity of the protein-like components C4 and C6, and the humic-like component C5, exhibited distinct pattern, as shown in Figure 13. In both regions, GGDW and OBDW, median fluorescence intensity values of C4, I_{C4}, corresponding to tryptophan, consistently decreased with depth, showing the highest values in SW ($I_{\mathrm{C4(GGDW)}} = 0.096$ R.U., $I_{\mathrm{C4(OBDW)}} = 0.091$ R.U.) and the lowest in BW ($I_{\mathrm{C4(GGDW)}} = 0.082$ R.U., $I_{\mathrm{C4(OBDW)}} = 0.077$ R.U.). Between BSWW and BW layers, no statistically significant differences were found. A similar trend was observed for the vertical distribution of the median fluorescence intensity values of C5, I_{C5}, with a substantial decrease in the BW layer. In the OBDW region, this decrease was statistically insignificant. The vertical distribution of the median fluorescence intensity values of C6, I_{C6}, corresponding to tyrosine, varied between the GGDW and OBDW. In the GGDW, the highest median fluorescence intensity of C6, was observed in SW, ($I_{\mathrm{C6(GGDW)}} = 0.028$ R.U.), then slightly decreased in BSWW ($I_{\mathrm{C6(GGDW)}} = 0.027$ R.U.) and BW ($I_{\mathrm{C6(GGDW)}} = 0.024$ R.U.) but those differences were not statistically significant. In the OBDW, the highest median fluorescence intensity of C6, was observed in SW ($I_{\mathrm{C6(OBDW)}} = 0.035$ R.U.), followed by a decrease in the BSWW ($I_{\mathrm{C6(OBDW)}} = 0.027$ R.U.), and then a slight increase in the BW ($I_{\mathrm{C6(OBDW)}} = 0.028$ R.U.). Only the difference between SW I BW layers was statistically significant.

The vertical median distribution of total fluorescence intensity, I_{tot}, in the Gulf of Gdańsk deep stations showed a distinctly different pattern compared to one the open Baltic deep stations (Figure 14). In the GGDW, surface waters exhibited the highest median I_{tot} ($I_{\mathrm{tot(GGDW)}} = 0.731$ R.U.) accompanied by a wide range of variability. As depth increased, there was a reduction in the median $I_{\mathrm{tot(GGDW)}}$ (but statistically insignificant) accompanied by a tightening of its variability range. In the OBDW, the median $I_{\mathrm{tot(OBDW)}}$, in surface water ($I_{\mathrm{tot(OBDW)}} = 0.648$ R.U.) was comparable to $I_{\mathrm{tot(OBDW)}}$ median values observed in Baltic Sea Winter

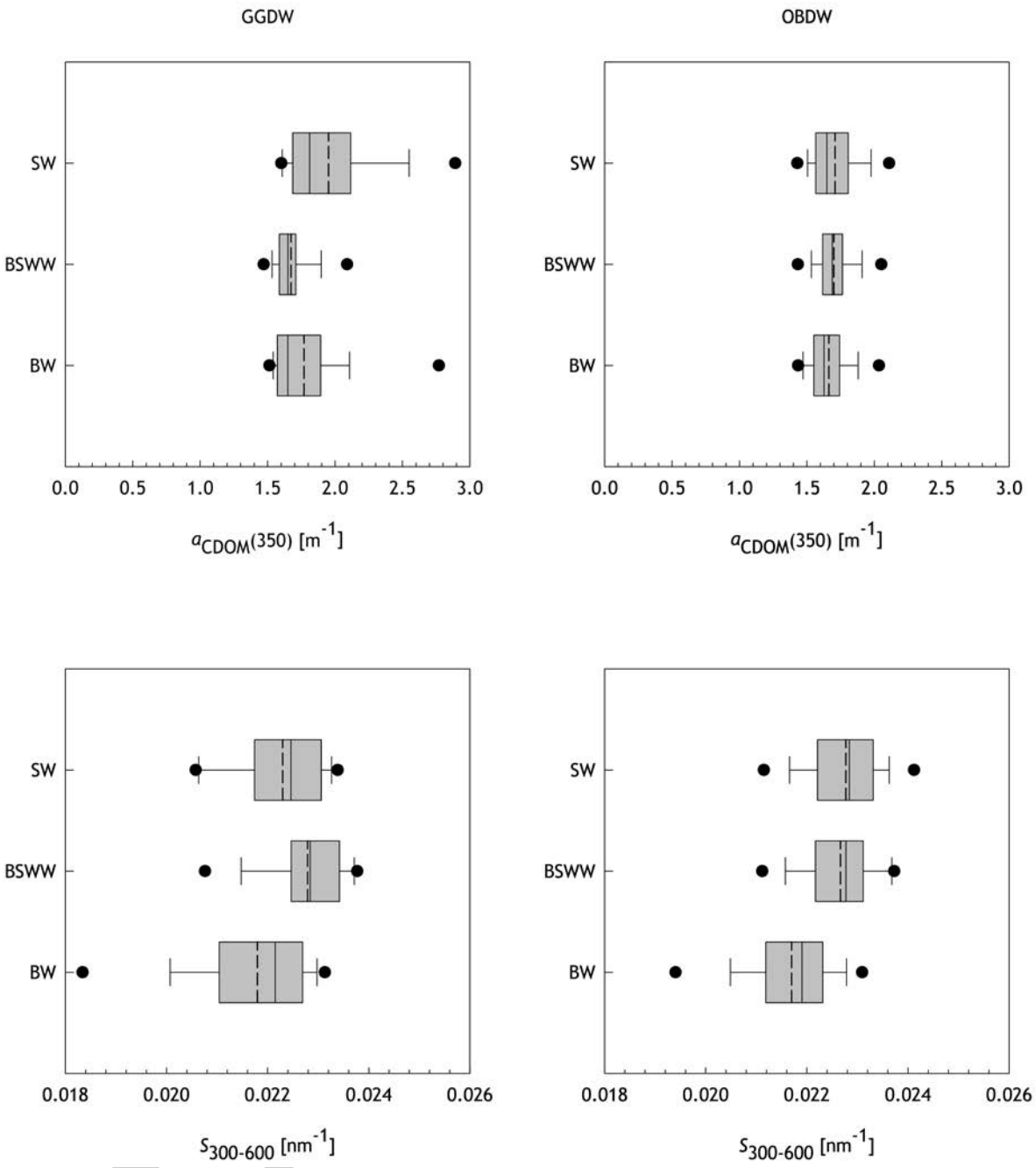

Figure 10. Median distribution of $a_{\mathrm{CDOM}}(350)$ and $S_{300-600}$ in different water layers in the Gulf of Gdańsk Deep Waters (GGDW) and the Open Baltic Deep Waters (OBDW). Median values are marked with the solid line, mean values are marked with the dashed line, 10th and 90th percentiles are marked with the whiskers, and 25th and 75th percentiles with the box. SW – Surface Water, BSWW – Baltic Sea Winter Water, BW – Bottom Water.

Water ($I_{\mathrm{tot(OBDW)}} = 0.649$ R.U.). Both medians were statistically lower than the one for Bottom Water ($I_{\mathrm{tot(OBDW)}} =$ 0.665 R.U.). The range of variability of $I_{\mathrm{tot(OBDW)}}$, in the OBDW was significantly smaller compared to the waters of the GGDW, particularly in surface water.

The humic-like components, predominantly contributing to the total fluorescence intensity of DOM, displayed a vertical distribution of the median of fluorescence intensity I_h, that closely followed the I_{tot} distribution, in both research areas (Figure 14). In the GGDW's surface waters, humic-like substances show highest values ($I_{h(\mathrm{GGDW})} =$ 0.575 R.U.), with the fluorescence intensity decreased in BSWW ($I_{h(\mathrm{GGDW})} = 0.561$ R.U.) and increased again in the BW ($I_{h(\mathrm{GGDW})} = 0.563$ R.U.). In the OBDW the highest me-

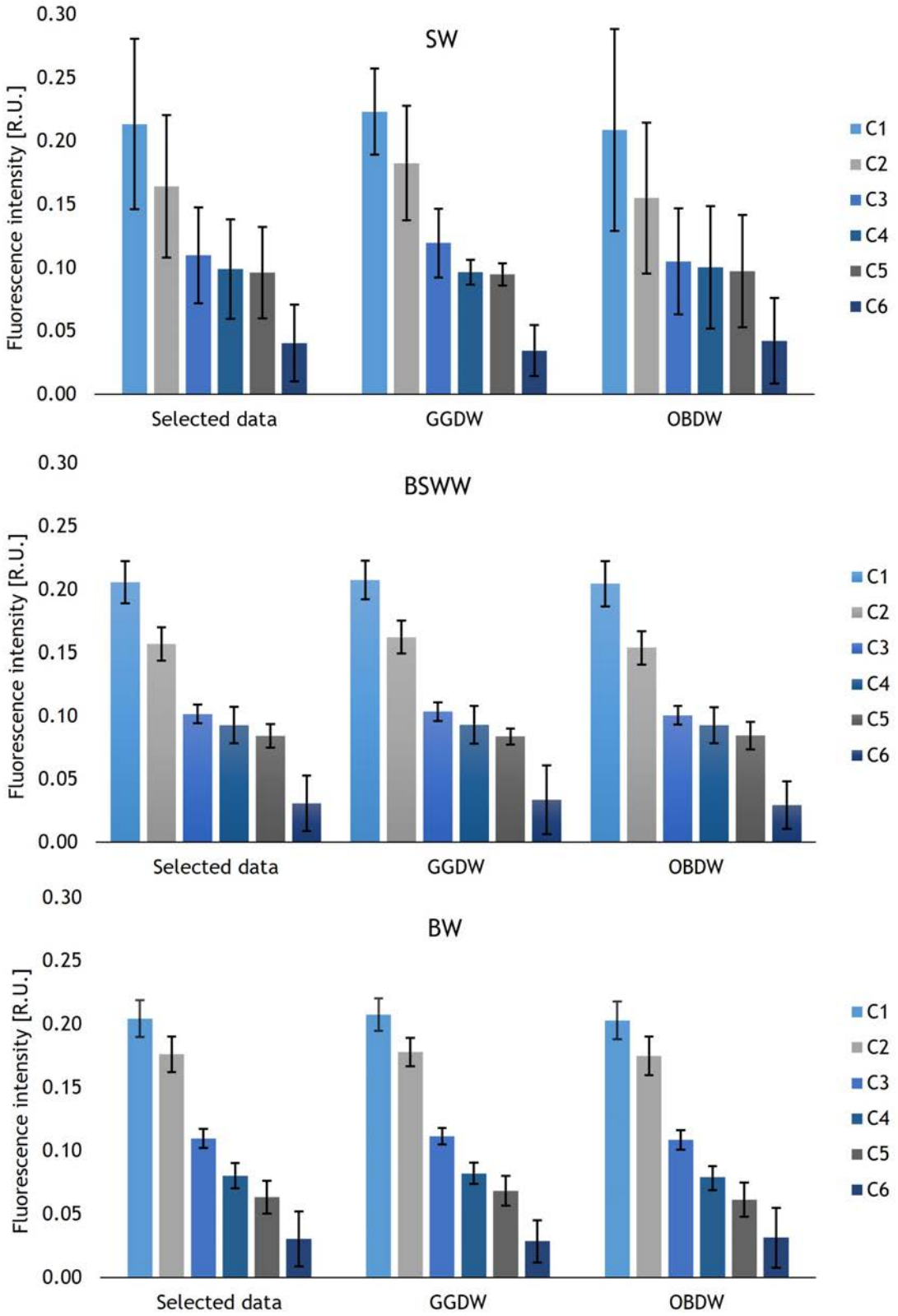

Figure 11. Composition of DOM fluorescence excitation/emission spectra in: Selected data set (70 stations), Gulf of Gdańsk Deep Waters (GGDW) and Open Baltic Deep Waters (OBDW) in years 2008–2013. Bar plots represent average fluorescence intensity of 6 identified components, whiskers represents the standard deviation.

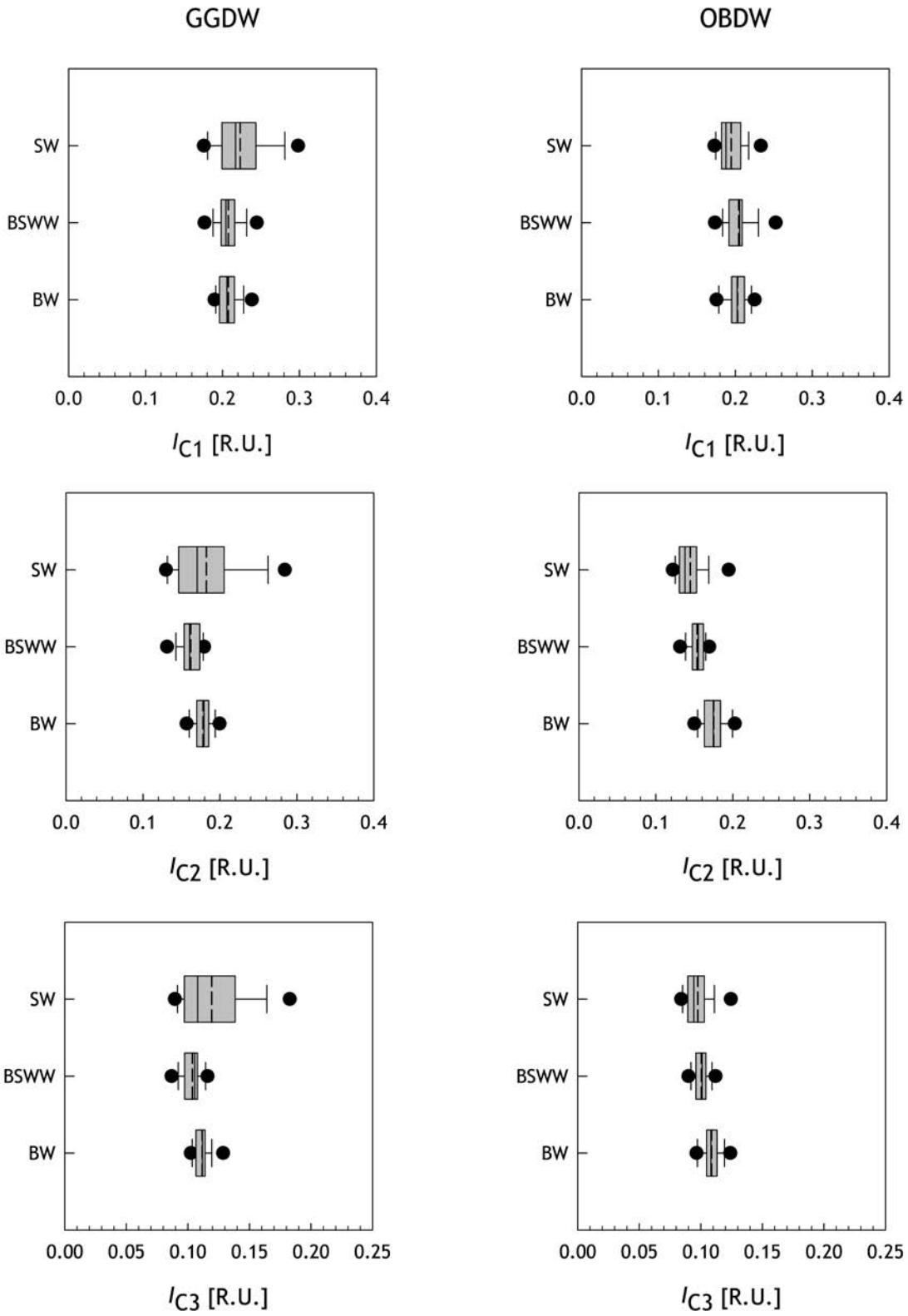

Figure 12. Median distribution of fluorescence intensity values of three identified by PARAFAC humic-like components: C1, C2, and C3 in different water layers in the Gulf of Gdańsk Deep Waters (GGDW) and the Open Baltic Deep Waters (OBDW). Median values are marked with the solid line, mean values are marked with the dashed line, 10th and 90th percentiles are marked with the whiskers, and 25th and 75th percentiles with the box. SW – Surface Water, BSWW – Baltic Sea Winter Water, BW – Bottom Water.

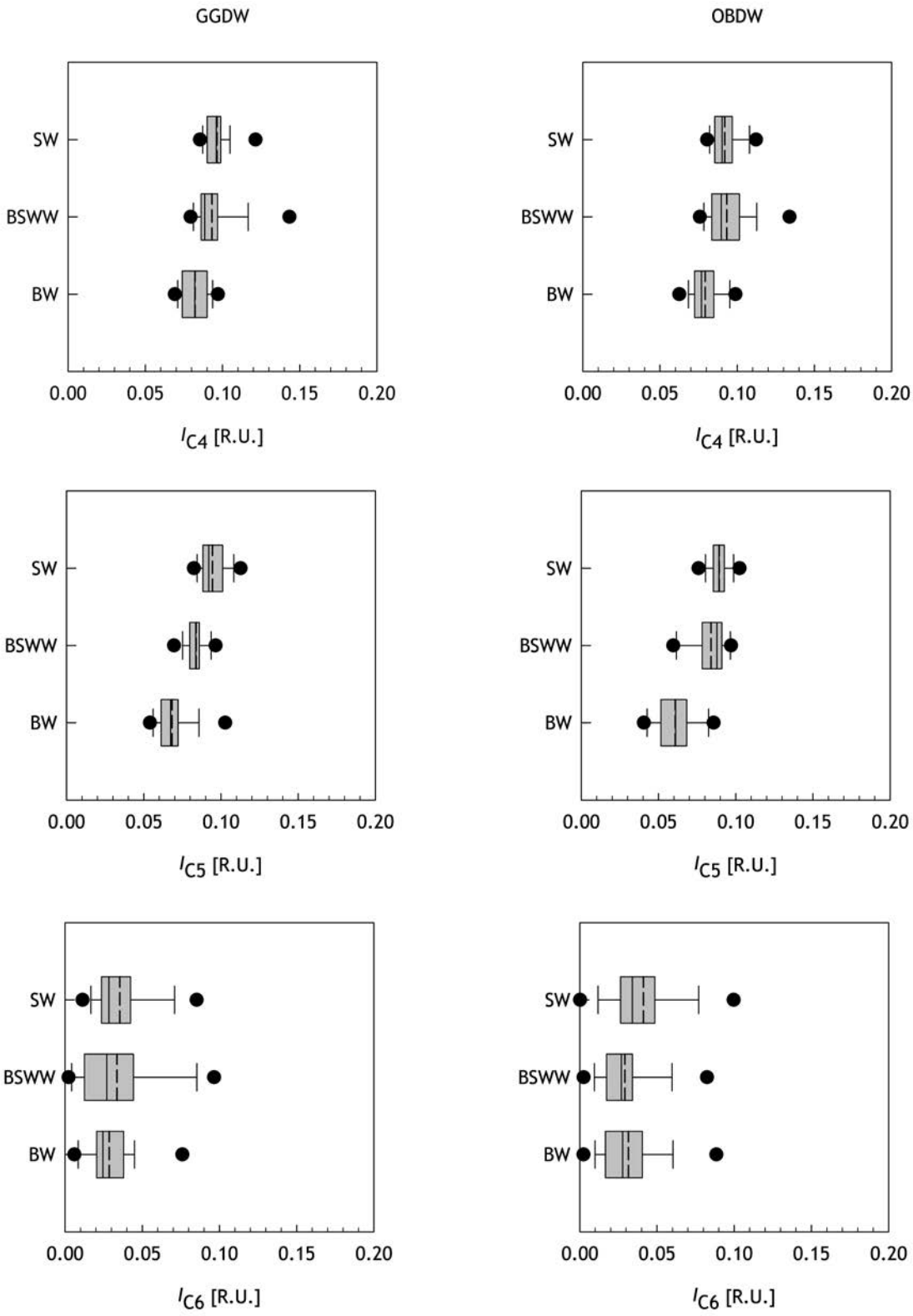

Figure 13. Median distribution of fluorescence intensity values of identified by PARAFAC one humic-like component: C5, and two protein-like components: C4, and C5 in different water layers in the Gulf of Gdańsk Deep Waters (GGDW) and the Open Baltic Deep Waters (OBDW). Median values are marked with the solid line, mean values are marked with the dashed line, 10th and 90th percentiles are marked with the whiskers, and 25th and 75th percentiles with the box. SW – surface Water, BSWW – Baltic Sea Winter Water, BW – Bottom Water.

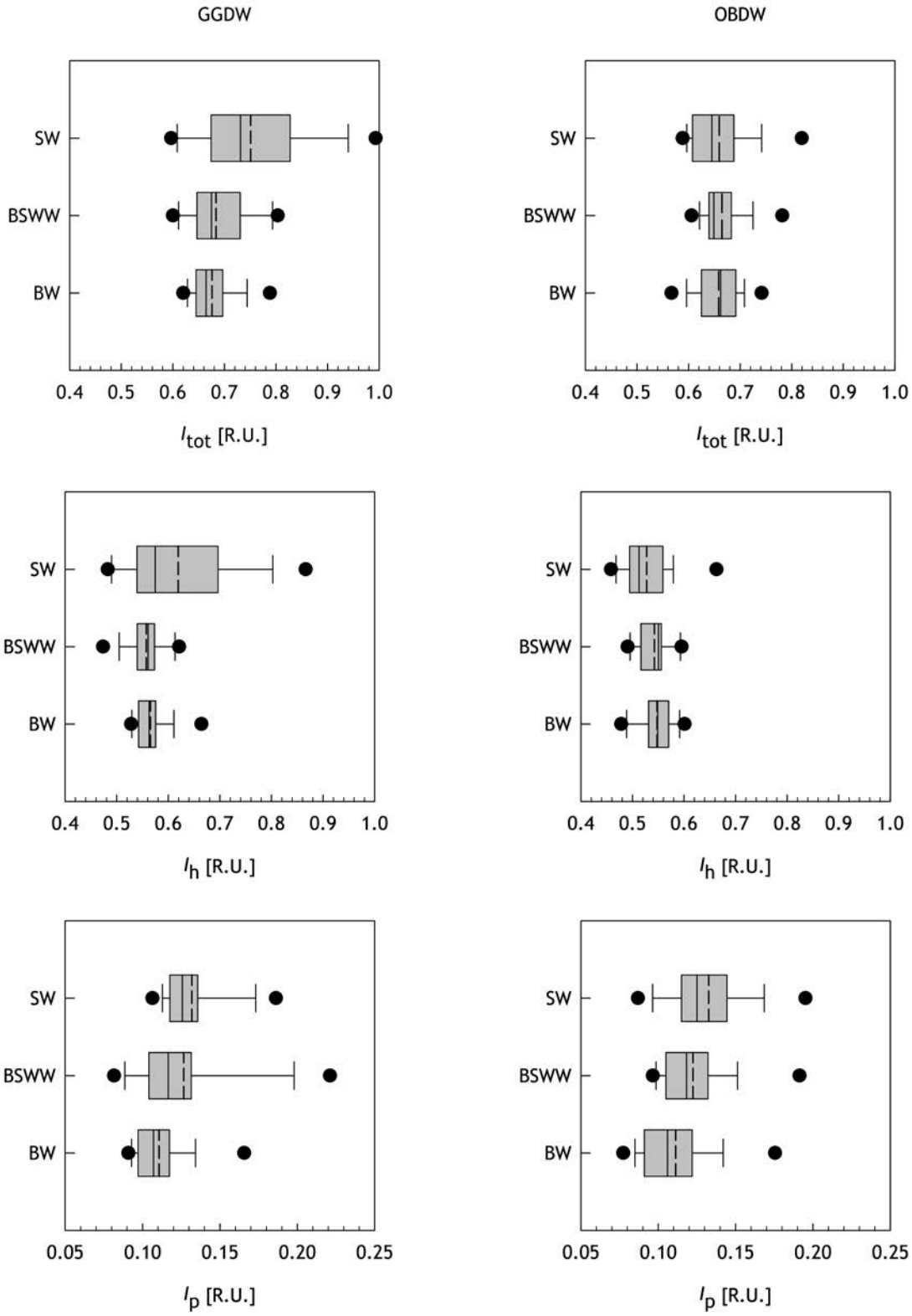

Figure 14. Median distribution of total fluorescence intensity values, Itot, along with fluorescence intensity values of humic-like, I_h, and protein-like, I_p, component: in different water layers in the Gulf of Gdańsk Deep Waters (GGDW) and the Open Baltic Deep Waters (OBDW). Median values are marked with the solid line, mean values are marked with the dashed line, 10th and 90th percentiles are marked with the whiskers, and 25th and 75th percentiles with the box. SW – Surface Water, BSWW – Baltic Sea Winter Water, BW – Bottom Water.

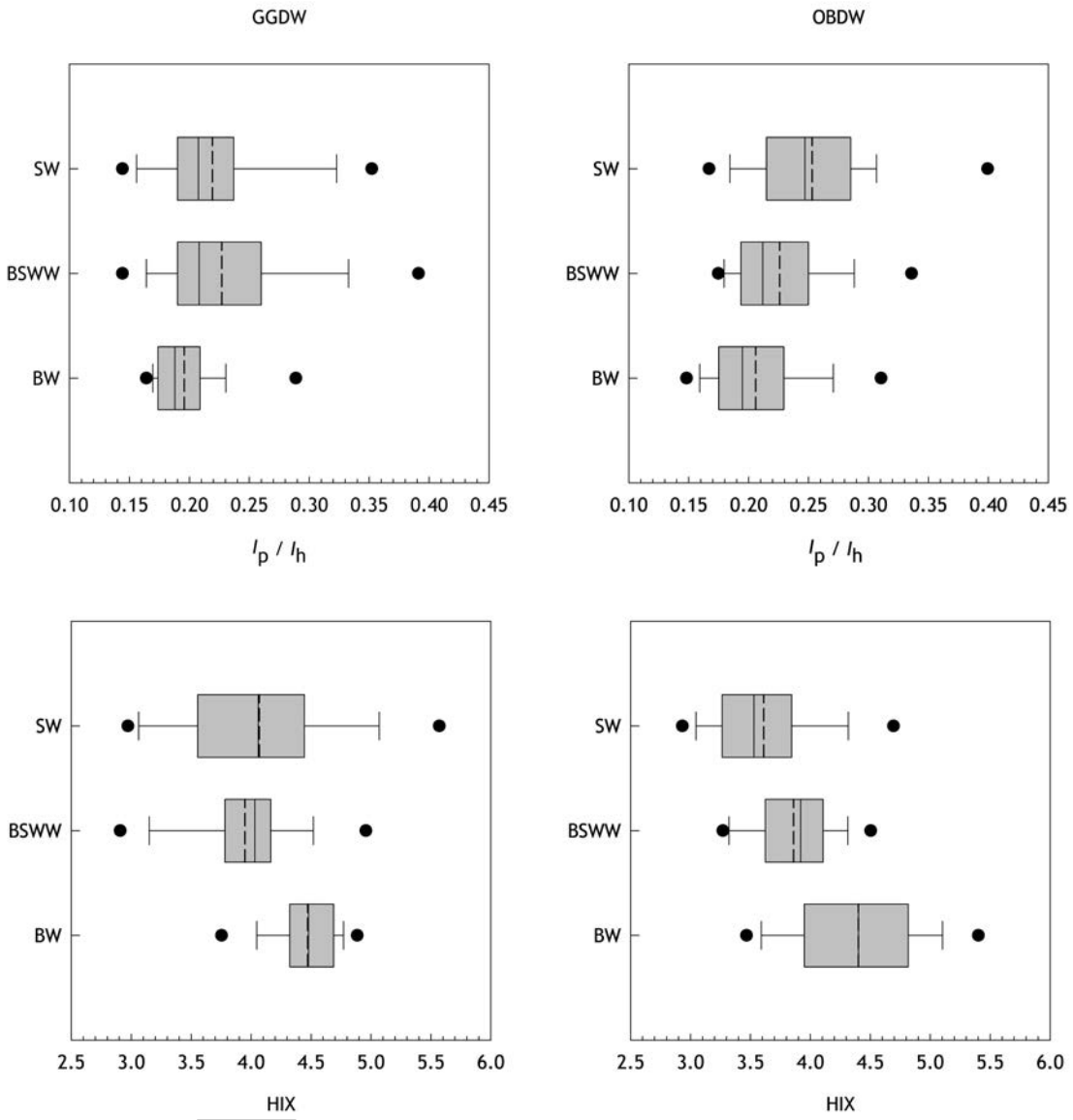

Figure 15. Median distribution of the sum of fluorescence intensity of identified protein-like components to the sum of fluorescence intensities of identified humic-like components ratio, I_p/I_h, and humification index, HIX: in different water layers in the Gulf of Gdańsk Deep Waters (GGDW) and the Open Baltic Deep Waters (OBDW). Median values are marked with the solid line, mean values are marked with the dashed line, 10th and 90th percentiles are marked with the whiskers, and 25th and 75th percentiles with the box. SW – Surface Water, BSWW – Baltic Sea Winter Water, BW – Bottom Water.

dian value of the humic-like substances was observed in BSWW ($I_{h(\mathrm{OBDW})} = 0.561$ R.U.), a slightly lower in BW ($I_{h(\mathrm{OBDW})} = 0.549$ R.U.) and the lowest ($I_{h(\mathrm{OBDW})} = 0.513$ R.U.) in surface waters. The vertical distribution of fluorescence intensity median values of the identified protein-like components, I_p, followed a similar trend in both GGDW and OBDW. These values were higher in SW ($I_{p(\mathrm{GGDW})} = 0.126$ R.U., $I_{p(\mathrm{OBDW})} = 0.127$ R.U.) and systematically decreased with depth, indicating substantial shift in the qualitative composition of DOM across different Baltic Sea regions.

Figure 15 presents the vertical distribution of median values of the I_p/I_h ratio and HIX index in GGDW and OBDW. In the GGDW, the highest median of I_p/I_h ($I_p/I_{h(\mathrm{GGDW})} = 0.228$) was observed in the BSWW and the lowest in the bottom water ($I_p/I_{h(\mathrm{GGDW})} = 0.196$). The OBDW showed a slightly different pattern with the highest I_p/I_h values in surface water ($I_p/I_{h(\mathrm{OBDW})} = 0.253$) and the lowest in bottom water ($I_p/I_{h(\mathrm{OBDW})} = 0.205$). The HIX index displayed an inverse trend to the I_p/I_h in both regions.

4. Discussion

Published measurements from the Baltic Sea and Danish Straits demonstrate that defining the range of variability of $a_{CDOM}(\lambda)$ and $S(\lambda-\lambda_0)$ is challenging (Kowalczuk, 1999; Stedmon et al., 2000; Højerslev and Aas, 2001; Kowalczuk et al., 2006; Berthon and Zibordi, 2010; Harvey et al., 2015). This challenge arises from the heterogeneity of the data presented. $a_{CDOM}(\lambda)$ coefficient is presented in the above publications at various wavelengths, while the $S(\lambda-\lambda_0)$ coefficient in different wavelength ranges. When focusing on one reported wavelength, $a_{CDOM}(375)$ values range from around 1 m^{-1} in open Baltic Sea waters, and around 0.8 m^{-1} in the Great and Little Belts and the Sund (Stedmon et al., 2000). The highest values of $a_{CDOM}(375)$ exceeded 10 m^{-1} in southern Baltic Sea low-salinity estuarine waters (Kowalczuk et al., 2006) decreasing linearly with increasing salinity. The spectral slope $S_{\lambda-\lambda_0}$ is influenced by the relative contribution of the two main fractions of CDOM: humic and fulvic acids (Carder et al., 1989), and is modified by the photodegradation and microbial transformation of DOM. During exposure to solar radiation, the CDOM absorption coefficient decreases, and the spectral slope coefficient increases (Moran et al., 2000; Vähätalo and Wetzel, 2008). Changes in the $S(\lambda-\lambda_0)$ are also influenced by the physical mixing of water masses of different optical properties (Stedmon and Markager, 2003; Xie et al., 2012). Therefore, during the transport of water from terrestrial to marine environment, along the increasing salinity gradient, the $S_{\lambda-\lambda_0}$ values increased.

Previous studies in the Baltic Sea region and adjacent estuaries highlighted the complexity and heterogeneity of FDOM composition and sources (Stedmon et al., 2003, 2007; Kowalczuk et al., 2005b; Reader et al., 2019; Loginova et al., 2024). These studies demonstrated that FDOM distribution follows salinity gradients and is influenced by both terrestrial and autochthonous sources. For example, Stedmon et al. (2003) identified five distinct FDOM components in the Horsens Fjord estuary, most of which were of terrestrial origin, while Stedmon et al. (2007) observed differences in the contribution of humic- and protein-like fractions between Gulf of Finland, Bothnian Bay and Danish Straits. Similarly, Kowalczuk et al. (2005a,b) found that protein-like fluorophores increase in relative intensity with salinity in southern Baltic waters. Our findings are consistent with this general pattern. We observed a decreasing contribution of humic-like substances with increasing salinity, while the absolute abundance of protein-like components did not show a clear salinity-dependent trend (Figure 6). However, their relative significance increased in more saline waters due to the concurrent decline in humic-like fluorescence. This supports the previously described salinity-driven shift from terrestrial-dominated to autochthonous DOM fluorescence signatures, although the protein-like fluorescence itself does not exhibit a distinct salinity-driven gradient. However, our data extend these observations by quantifying this shift using spectral indices (e.g., HIX, SUVA(254), I_p/I_h) and by providing seasonal and vertical resolution across distinct water masses of the Baltic Sea.

Presented data set indicated a predominant contribution of humic-like substances of terrestrial and marine-terrestrial origin to the qualitative composition of the mixture of organic compounds forming FDOM within the southern Baltic Sea. The influence of local sources of FDOM in the form of autochthonous production of protein-like fluorophores becomes apparent further offshore and away from the sources of terrestrial organic matter inflow. Open water exhibits a higher proportion of biologically derived components (C4 + C6) compared to GCW. We observed that the increase in the fluorescence intensity of protein-like components was much smaller than the overall decrease in total FDOM fluorescence. This pattern is consistent with previous observations from the Baltic Sea (Kowalczuk et al., 2005b). That also aligns with the general trend of increasing significance of protein-like substances in marine and oceanic waters, especially those distant from the influence of freshwater inputs (Murphy et al., 2008; Kowalczuk et al., 2009).

The spectral indices, HIX and SUVA(254), and the I_p/I_h ratio, are appropriate tools for analyzing the sources and transformation processes of FDOM in the Baltic Sea waters. An increase in the proportion of humic acids, characterized by a large number of aromatic rings, in the FDOM mixture expands the spectral range of interactions of the FDOM mixture with electromagnetic radiation, simultaneously shifting the maximum intensity of fluorescence toward longer wavelengths (Zsolnay et al., 1999). In our study, HIX was characterized by a wide range of variability, from values below 3, typical for waters dominated by biologically derived DOM, to values indicating a large proportion of land-derived DOM (>15) (Huguet et al., 2009). This wide range of variability is typical for waters with salinity <7 (Huguet et al., 2009). Figure 16 shows the distribution of $S_{300-600}$ as a function of HIX and salinity. Low $S_{300-600}$ values were associated with low salinity and high HIX, typical for DOM of riverine origin (Zsolnay et al., 1999, Huguett et al., 2009). A decrease in HIX values in waters with higher salinity corresponded with an increase in $S_{300-600}$ values. The observations confirm the relationship between the CDOM absorption spectral slope coefficient and the qualitative composition of DOM in terms of aromaticity (Carder et al., 1999). The statistical relationship between HIX and $S_{300\text{-}600}$ was approximated by a non-linear, exponential, inverse proportional function characterized by high correlation and determination coefficients (R = 0.71, Table 4), although the data show a considerable dispersion. The variability results from regional differences in DOM sources, transformation processes, and environmental conditions. A similar relationship between these spectral indices was described in the Atlantic Ocean

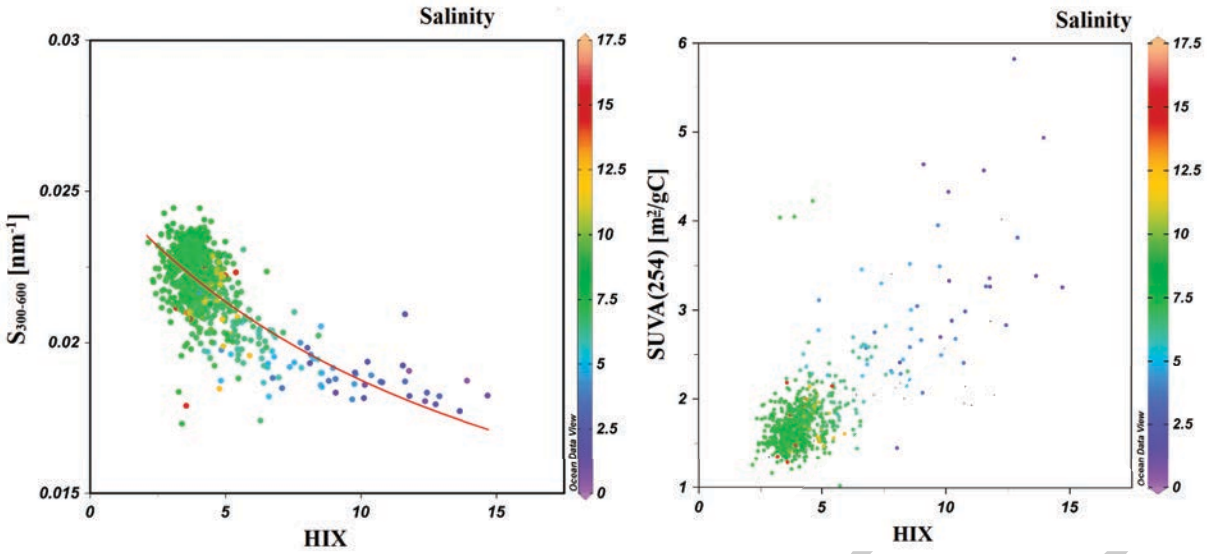

Figure 16. Distribution of the CDOM absorption slope coefficient, $S_{300-600}$ and the carbon specific absorption coefficient, SUVA(254), in relation to the Humification Index (HIX). Color bars show salinity of the samples.

by Kowalczuk et al. (2013).

Areas characterized by low HIX values are generally associated with areas of high I_p/I_h values (Huguet et al., 2009; Kowalczuk et al., 2013),whereas high HIX values combined with low I_p/I_h ratios clearly indicate the dominance of the humic-like substances in the FDOM pool. The spatial variability of both indices in the Baltic Sea is consistent with observations from other marine and oceanic basins. In the Baltic Sea, the spatial variability of HIX and I_p/I_h reflects distance from the freshwater sources, periods and regions of enhanced biological production, and the extent of FDOM transformation and degradation (e.g. Terzić et al., 2024). In the GGDW, higher HIX values and lower I_p/I_h values were observed compared to those found in OBDW (Figure 15). Apart from spatial variability, both described indices exhibited seasonal variability. In the GCW, a twofold increase in the median values of the HIX was observed from February (minimum) to April, while I_p/I_h showed the opposite pattern with maximum values in February and minimum in April. These changes coincided with periods of enhanced freshwater inflow and spring phytoplankton blooms, indicating an increased dominance of the humic-like fraction in the FDOM pool (Huguet et al., 2009; Kowalczuk et al., 2013). A similar seasonal variability of the HIX was observed by Huguet et al. (2009) in the Gironde River estuary (southwestern France) in waters with salinity <15, where the increase in HIX values also coincided with the periods of intensified river discharge. It is important to note that the spring decline in I_p/I_h reflected a shift in the relative composition of the FDOM pool rather than a reduction in the absolute abundance of protein-like fluorophores. This slight increase in I_p/I_h observed in May suggests that, following the spring runoff peak, locally produced autochthonous DOM begins to contribute more visibly to the protein-like fraction. The comparison of the annual cycle of total DOM fluorescence with the seasonal variability of the Vistula River discharge (Figure S1) and with the annual dynamics of chlorophyll *a* (Figure S2) further indicates that the GCW fluorescence regime is jointly shaped by terrestrial DOM inflow and by local FDOM production associated with phytoplankton and cyanobacterial blooms. In the open Baltic waters, the stability of $I_p/I_{h(\mathrm{OW})}$ medians in the first months of the year coincided with the similarly stable values of total fluorescence. This suggests that autochthonous DOM production in winter and early spring was in near-equilibrium with the inflow of terrestrial DOM, maintaining a relatively constant FDOM composition despite seasonal changes in hydrological forcing. The increase in $I_p/I_{h(\mathrm{OW})}$ in late summer and early fall was likely driven by intensified autochthonous DOM production during cyanobacterial blooms. Post-bloom transformation and reworking of this organic matter may further contribute to the accumulation of both protein-like and newly formed humic-like FDOM, as previously noted for Baltic and temperate coastal systems (Stedmon and Markager, 2005).

The vertical distribution of fluorescence intensities of humic-like and protein-like components in GGDW and OBDW stations reflected intensities of various processes shaping the qualitative composition of FDOM across different water layers. In the GGDW, the inflow of terrigeneous dissolved organic matter from the Vistula River (Figure S1) significantly increased I_{tot} and I_h in the surface waters. The constant inflow from the Vistula River catchment area compensated the decrease of I_{tot} and I_h intensities in this layer, due to photochemical processes and dilution of freshwater

through mixing with marine water. In the surface layer of the OBDW the decrease in I_{tot} and I_h resulted mainly from photochemical reaction, as the dilution effect was less pronounced due to less intensive mixing. The prolonged water retention time in this region, coupled with a generally lower absorption and higher transparency of the waters, favor the accumulation of FDOM degradation products in the mixed layer (Terzić et al., 2024). Experiments and observations showed that humic-like substances are very susceptible to photochemical decomposition (Grzybowski, 2000; Stedmon et al., 2007), resulting predominantly in dissolved organic compounds with low molecular weight and spectral characteristics of excitation and emission fluorescence similar to the identified protein-like substances. Another factor contributing to the accumulation of low molecular weight DOM was the autochthonous production by the autotrophic protist community. Studies in Arctic and Baltic Sea waters conclusively demonstrated that an increase in phytoplankton biomass directly contributes to the pool of protein-like substances in the mixed layer (Yamashita et al., 2007; Makarewicz et al., 2018). Terzić et al. (2024) reported a statistically significant relationship ($R = 0.77$) between $a_{\mathrm{LH}}(676)$ and FDOM-Ch3 (the fluorescence intensity of the protein-like fraction of FDOM) in surface waters of the Baltic Sea. A similar dynamic was found in the Baltic Sea surface waters, where a statistically significant correlation was observed between CDOM absorption coefficient and the concentration of chlorophyll *a* (Kowalczuk et al., 2006; Meler et al., 2018). The cumulative effect of phytoplankton production, photochemical and microbial degradation of the humic-like fraction enhanced by mixing of seawater and freshwater, leads to an increase in I_p which is particularly noticeable in the surface layer of the Baltic Proper.

Winter convective mixing leads to vertical homogenization of concentrations of optically active components in the marine water column, coinciding with the decline in phytoplankton activity in the surface layer and a seasonal reduction in freshwater inflow into the Baltic Sea. This process results in reduction of magnitude of the coefficients describing optical properties of seawater (Sagan, 2008; Kratzer and Moore, 2018). As a consequence, a decrease in the fluorescence intensities of humic-like substances, I_h, was observed in the GGDW stations, while a slight increase was recorded in the OBDW, both within the Baltic Sea Winter Water layer. This modest increase in I_h within the BSWW may result from microbiological transformations of DOM, leading to an increased concentration of FDOM components with spectral characteristics resembling humic-like substances (Terzić et al., 2024). Furthermore, the isolation of BSWW from the biological and photochemical processes occurring in the surface layer results in a reduction in the concentrations of protein-like components, serving as substrates for the growth of microheterotrophs. The Baltic Sea Deep Water originates from surface waters of the Danish Straits that are transported into the deeper parts of the basin during periodic inflow events. The higher temperatures observed below the permanent pycnocline, compared to those observed below the overlying BSWW, reflect long-term shifts in the inflow regime. In recent decades, the frequency of major winter inflow events has decreased, while irregular baroclinic intrusions of saltier and typically warmer Kattegat waters have become more common, resulting in warming the deep layer. In contrast, the waters entering the GGDW through the Słupsk Channel lose heat while mixing with the overlying water masses, leading to lower temperatures in this region. These waters, characterized by significantly lower DOC concentrations and lower CDOM light absorption coefficients, show a linear decrease in both parameters with increasing salinity (Stedmon et al., 2007; Osburn and Stedmon, 2011). Therefore, the optical characteristics of the Baltic Sea's deep waters should reflect those prevailing in the Danish Straits, adjusted for the corresponding salinity levels. Our data indicated an increase in the fluorescence intensity of humic-like components in deep waters, exceeding levels observed in BSWW, despite higher salinity. Studies by Kowalczuk et al. (2015) and Terzić et al. (2024) demonstrated that in anoxic deep waters, the diffusion of DOM from seabed sediments leads to an increase in humic-like fluorescence and elevated $a_{\mathrm{CDOM}}(350)$. These studies also showed that microbial processes in oxygen-depleted bottom waters can reduce the fluorescence intensity of protein-like DOM, I_p. Together, these mechanisms alter the qualitative composition of DOM in deep waters. With increasing depth, the proportion of humic-like substances in FDOM increases, as reflected by a decrease in the I_p/I_h ratio, particularly evident in the OBDW. Deep waters are further enriched in saturated polycyclic dissolved organic compounds, which is supported by higher HIX values and an increase in the CDOM absorption spectrum slope coefficient.

5. Conclusions

Our comprehensive six-year study in the southern Baltic Sea, has provided significant insights into the spatial and seasonal variability of Fluorescent Dissolved Organic Matter. The application of parallel factor analysis (PARAFAC) has enabled the identification of six distinct FDOM components of terrestrial and marine origin and revealed consistent spatial patterns driven largely by the riverine input from the Vistula River.

Our results confirm the importance of freshwater inflow in shaping the distribution of allohthonous DOM, especially in coastal areas and during spring. In contrast, open waters showed a more balanced DOM composition and seasonality, with protein-like substances becoming relatively more abundant later in the year. Vertical profiles further indicate the enrichment of the bottom waters of the open Baltic in humic-like components, while the sur-

face layer near the river mouth remained enriched due to constant input riverine water, balancing its loss due to photodegradation.

The findings underscore the role of DOM in modulating the optical and biogeochemical properties of semi-enclosed seas such as the Baltic. The strong coupling between hydrological conditions, DOM origin, and its spectral properties demonstrates the sensitivity of the system to both natural and anthropogenic changes.

Our findings highlight the utility of optical methods and PARAFAC modeling in characterizing DOM sources and dynamics. Future studies should focus on long-term monitoring programs and further explore links between DOM composition, microbial activity, and carbon cycling. Such efforts are essential for understanding and predicting the role of coastal and marginal seas in global carbon budgets under changing environmental conditions.

Acknowledgements

This work was funded by the National Science Centre project PRELUDIUM awarded to MZ (contract no. UMO-2012/05/N/ST10/03648). P.K. was partially funded by National Science Centre project OPUS17 (contract no. UMO-2019/33/B/ST10/01232) and Statutory Research Programme II.5.

Supplementary material

Supplementary material associated with this article can be found here.

Conflict of interest

None declared.

References

Babin, M., Stramski, D., Ferrari, G.M., Claustre, H., Bricaud, A., Obolensky, G., Hoepffner, N., 2003. *Variations in the light absorption coefficients of phytoplankton, nonalgal particles, and dissolved organic matter in coastal waters around Europe*. J. Geophys. Res. 108 (C7), 3211. https://doi.org/10.1029/2001JC000882

Berthon, J.-F., Zibordi, G., 2010. *Optically black waters in the northern Baltic Sea Geophys*. Res. Lett. 37 (9), L09605. https://doi.org/10.1029/2010GL043227

Cahill. B.E., Kowalczuk, P., Kritten, L., Gräwe, U., Wilkin, J., Fischer, J., 2023. *Estimating the seasonal impact of optically significant water constituents on surface heating rates in the western Baltic Sea*. Biogeosciences, 20 (13), 2743–2768.

Carder, K.L., Chen, F.R., Lee, Z.P., Hawes, S.K., Kamykowski, D., 1999. *Semianalityc moderate-resolution imaging spectrometer algorithms for chlorophyll a and absorption with bio-optical domains based on nitrate-depletion temperatures*. J. Geophys. Res. 104, C3, 5403–5421. https://doi.org/10.1029/1998JC900082

Carder, K.L., Steward, R.G., Harvey, G.R., Ortner, P.B., 1989. *Marine humic and fulvic acids: Their effects on remote sensing of ocean chlorophyll*. Limnol. Oceanogr. 34, 68–81.

Catalá, T.S., Álvarez-Salgado, X.A., Otero, J., Iuculano, F., Companys, B., Horstkotte, B., 2016. *Drivers of fluorescent dissolved organic matter in the global epipelagic ocean*. Limnol. Oceanogr. 61 (3), 1101–1119.

Coble, P.G., 1996. *Characterization of marine and terrestrial DOM in seawater using excitation – emission matrix spectroscopy*. Mar. Chem. 51, 325–346.

Drozdowska, V., 2007a. *Seasonal and spatial variability of surface seawater fluorescence properties in the Baltic and Nordic Seas: results of lidar experiments*. Oceanologia, 49 (1), 59–69.

Drozdowska, V., 2007b, *The lidar investigation of the upper water layer fluorescence spectra of the Baltic Sea*. Eur. Phys. J. Spec. Top. 144, 141–145.

Drozdowska, V., Kowalczuk, P., Konik, M., Dzierzbicka-Glowacka, L., 2018. *Study on Different Fractions of Organic Molecules in the Baltic Sea Surface Microlayer by Spectrophoto – and Spectrofluorimetric Methods. Frontiers in Marine Science*. Sec. Marine Biogeochem. 5. https://doi.org/10.3389/fmars.2018.00456

Ferrari, G., Dowell, M., 1998. *CDOM absorption characteristics with relation to fluorescence and salinity in coastal areas of the southern Baltic Sea*. Estuar. Coast. Shelf S. 47 (1) 91–105.

Ferrari, G., Tassan, S., 1991. *On the accuracy of determining light absorption by "yellow substance" through measurement of induced fluorescence*. Limnol. Oceanogr. 36 (4), 777–786.

Friedlingstein, P., O'Sullivan, M., Jones, M.W., et al., 2025. *Global Carbon Budget 2024*. Earth Sys. Sci. Data, 16 (8), 965–1039. https://doi.org/10.5194/essd-17-965-2025

Grzybowski, W., 2000. *Effect of short-term sunlight irradiation on absorbance spectra of chromophoric organic matter dissolved in coastal and riverine water*. Chemosphere, 40, 1313–1318.

Hansell, D.A, Carlson, C.A., 2001. *Marine Dissolved Organic Matter and the Carbon Cycle*. Oceanography, 14 (4), 41–49. https://doi.org/10.5670/oceanog.2001.05

Hansell, D.A., 2013. *Recalcitrant Dissolved Organic Carbon Fractions*. Annu. Rev. Mar. Sci. 5, 421–445. https://doi.org/10.1146/annurev-marine-120710-100757

Hansell, D.A, Carlson, C.A., Repeta, D.J., Schliitzer, R., 2009. *Dissolved organic matter in the ocean: new insights stimulated by a controversy*. Oceanography, 22, 52–61.

Harshman, R.A., 1984. *How can I know if it's real? A catalog of diagnostics for use with three-model factor analysis*

and multidimensional scaling. [In:] Law H.G, Snyder Jr.C.W., Hattie J.A., McDonald R. (Eds.), *Research Methods for multimode data analysis*. Preager, New York, 566–591.

Harvey, E.T., Kratzer, S., Andersson, A., 2015. *Relationships between colored dissolved organic matter and dissolved organic carbon in different coastal gradients of the Baltic Sea*. Ambio 44 (Suppl. 3), 392–401. https://doi.org/10.1007/s13280-015-0658-4

Højerslev, N.K., Aas, E., 1991, *A relationship for the penetration of ultraviolet Bradiation into the Norwegian Sea*, J. Geophys. Res. 96, 17003–17005.

Huguet, A., Vacher, L., Relexans, S., Saubusse, S., Froidefond, J.M., Parlanti, E., 2009. *Properties of fluorescent dissolved organic matter in the Gironde estuary*. Org. Geochem. 40 (6), 706–719.

IMGW-PIB (Institute of Meteorology and Water Management – National Research Institute), 2023. *Hydrological data – Vistula River discharge (2008–2013)*. Retrieved from https://danepubliczne.imgw.pl [Accessed: 30 Sep 2025].

Jerlov, N.G., 1976. *Marine Optics*. Elsevier Oceanography Series, Elsevier, Amsterdam, 230 pp.

Jiao, N., Herndl, G.J., Hansell, D.A., Benner, R., Kattner G., Wilhelm, S.W., Kirchman, D.L., Weinbauer, M.G., Luo, T., Chen F., Azam, F., 2010. *Microbial production of recalcitrant dissolved organic matter: long-term carbon storage in the global ocean*. Nat Rev Microbiol. 8 (8), 593–599. https://doi.org/10.1038/nrmicro2386

Jiao, N., Herndl, G.J., Hansell, D.A., Benner, R., Kattner, G., Wilhelm, S.W., 2011. *The microbial carbon pump and the oceanic recalcitrant dissolved organic matter pool*. Nat. Rev. Microbiol. 9, 555–555. https://doi.org/10.1038/nrmicro2386-c5

Jørgensen, L., Stedmon, C.A., Kragh, T., Markager, S., Middelboe, M., Sondergaard, M., 2011. *Global trends in the fluorescence characteristics and distribution of marine dissolved organic matter*. Mar. Chem. 126, 139–148.

Kowalczuk, P., 1999, *Seasonal variability of yellow substance absorption in the surface layer of the Baltic Sea*. J. Geophys. Res. 104 (C12), 30047–30058.

Kowalczuk, P., Durako, M.J., Young, H., Kahn, A.E., Cooper, W.J., Gonsior, M., 2009. *Characterization of dissolved organic matter fluorescence in the South Atlantic bight with use of PARAFAC model: interannual variability*. Mar. Chem. 113, 182–196.

Kowalczuk, P., Olszewski, J., Darecki, M., Kaczmarek, S.M., 2005a. *Empirical relationship between coloured dissolved organic matter (CDOM) absorption and apparent optical properties in Baltic Sea waters*. Int. J. Remote Sens. 26, 2, 345–370. https://doi.org/10.1080/01431160410001720270

Kowalczuk, P., Sagan, S., Olszewski, J., Darecki, M., Hapter, R., 1999. *Seasonal changes in selected optical parameters in the Pomeranian Bay in 1996–1997*. Oceanologia 41 (3), 309–334.

Kowalczuk, P., Sagan, S., Zabłocka, M., Borzycka, K., 2015. *Mixing anomaly in deoxygenated Baltic Sea deeps indicates benthic flux and microbial transformation of chromophoric and fluorescent dissolved organic matter*. Estuar. Coast. Shelf Sci. 163, Pt. B, 206–217. https://doi.org/10.1016/j.ecss.2015.06.027

Kowalczuk, P., Stedmon, C.A., Markager, S., 2006, *Modeling absorption by CDOM in the Baltic Sea from season, salinity and chlorophyll*. Mar. Chem. 101, 1–11.

Kowalczuk, P., Stoń-Egiert, J., Cooper, W.J., Whitehead, R.F., Duralo, M.J., 2005b. *Characterization of chromophoric dissolved organic matter (CDOM) in the Baltic Sea by excitation emission fluorescence spectroscopy*. Mar. Chem. 96 (3–4), 273–292. https://doi.org/10.1016/j.marchem.2005.03.002

Kowalczuk, P., Tilstone, G.H., Zabłocka, M., Röttgers, R., Thomas, R., 2013, *Composition of dissolved organic matter along an Atlantic Meridional Transect from fluorescence spectroscopy and Parallel Factor Analysis*. Mar. Chem., 157, 170–184.

Kowalczuk, P., Zabłocka, M., Sagan, S., Kuliński, K., 2010. *Fluorescence measured in situ as a proxy of CDOM absorption and DOC concentration in the Baltic Sea*. Oceanologia 52 (3), 431–471. https://doi.org/10.5697/oc.52-3.431

Kratzer, S., Moore, G., 2018. *Inherent optical properties of the Baltic Sea in comparison to other seas and ocean*. Remote Sens. 10 (418). https://doi.org/10.3390/rs10030418

Leppäranta, M., Myrberg, K., 2009. *Physical Oceanography of the Baltic Sea*. Springer , Chichester, UK, 378 pp. https://doi.org/10.1007/978-3-540-79703-6

Loginova, A.N., Wunsch, U., Zabłocka, M., Cherkasheva, A., Szymczycha, B., Kuliński, K., Winogradow, A., Kowalczuk, P., 2024. *Qualitative variability of dissolved organic matter in the Baltic Sea sediments apparent from fluxes and optical properties*. Front. Mar. Sci. 11, 1433199. http://doi.org/10.3389/fmars.2024.1433199

Lønborg, C., Carreira, C., Abril, G., et al., 2024. *A global database of dissolved organic matter (DOM) concentration measurements in coastal waters (CoastDOM v1)*. Earth System Science Data, https://www.earth-system-science-data.net. https://doi.org/10.5194/essd-16-1107-2024 Lønborg, C., Fuentes-Santos, I.F., Carreira, C., et al., 2025. *Dissolved Organic Carbon in Coastal Waters: Global Patterns, Stocks and Environmental Physical Controls*. Global Biogeochem. Cy. 39 (5), e2024GB008407. https://doi.org/10.1029/2024GB008407

Lønborg, C., Carreira, C., Jickells, T., Álvarez-Salgado, X.A., 2020. *Impacts of Global Change on Ocean Dissolved Organic Carbon (DOC) Cycling*. Front. Marine Sci., 7,

466.
https://doi.org/10.3389/fmars.2020.00466

Meler, J., Woźniak, S.B., Stoń-Egiert, J., Woźniak, B., 2018, *Parametrization of phytoplankton spectral absorption coefficient in the Baltic Sea: general, monthly and two-component variants of approximation formulas*. Ocean. Sci., 14, 1523–1545.

Makarewicz, A., Kowalczuk, P., Sagan, S., Granskog, M.A., Pavlov, A.K., Zdun, A., Borzycka, K., Zabłocka, M., 2018, *Characteristics of chromophoric and fluorescent dissolved organic matter in the Nordic Seas*. Ocean Sci., 14, 543–562.

Moran, M.A., Sheldon, W.M., Zepp, R.G., 2000. *Carbon loss and optical property changes during long-term photochemical and biological degradation of estuarine dissolved organic matter*. Limnol. Oceanogr. 45, 1254–1264.
https://doi.org/10.4319/lo.2000.45.6.1254

Murphy, K.R., Buttler, K.D., Spencer, R.G.M., Stedmon, C.A., Boehme, J.R., Aiken, G.R., 2010. *Measurements of Dissolved Organic Matter Fluorescence in Aquatic Environments: An Interlaboratory Comparison*. Environ. Sci. Technol., 44, 9405–9412.

Murphy, K.R., Stedmon, C.A., Graeber, D., Bro, R., 2013. *Fluorescence spectroscopy and multi-way techniques*. PARAFAC. Anal. Methods, 5, 6557–6566.

Murphy, K.R., Stedmon, C.A., Waite, T.D., Ruiz, G.M., 2008. *Distinguishing between terrestrial and autochthonous organic matter sources in marine environments using fluorescence spectroscopy*. Mar. Chem., 108, 40–58.

Murphy, K.R., Stedmon, C.A., Wenig, P., Bro, R., 2014.]it OpenFluor-A spectral database of auto-fluorescence by organic compounds in the environment. Anal. Methods-UK, 6, 658–661.

Nelson, B.N., Siegel, D.A., Carlson, C.A., Swan, C.M., 2010. *Tracing global biogeochemical cycles and meridional overturning circulation using chromophoric dissolved organic matter*. Geophys. Res. Lett. 37, L03610.
https://doi.org/10.1029/2009GL042325

Nelson, B.N., Siegel, D.A., 2013. *The Global Distribution and Dynamics of Chromophoric Dissolved Organic Matter*. Annu. Rev. Mar. Sci. 5, 447–476.

Olszewski, J., Sagan, S., Darecki, M., 1992. *Spatial and temporal chan ges in some optical parameters in the southern Baltic*. Oceanologia, 33, 87–103.

Osburn, C.L., Stedmon, C.A., 2011. *Linking the chemical and optical properties of dissolved organic matter in the Baltic-North Sea transition zone to differentiate three allochtonus inputs*. Mar. Chem. 126 (1–4), 281–294.

Opsahl, S., Benner, R., 1997. *Distribution and cycling of terrigenous dissolved organic matter in the ocean*. Nature 386, 480–482.
https://doi.org/10.1038/386480a0

Roesler, C.S., Barnard, A., 2013. *Optical proxy for phytoplankton biomass in the absence of photophysiology: Rethinking the absorption line height*. Method. Oceanogr. 7, 79–94.
https://doi.org/10.1016/j.mio.2013.12.003

Sagan, S., 1991. *Transmisja światła w wodach południowego Bałtyku*. Rozpr. Monogr. 2/1991, Institute of Oceanology Polish Academy of Science, Sopot, 149 pp.

Sagan, S., 2008. *Rzeczywiste właściwości optyczne wód Bałtyku*. Rozpr. Monogr. 21/2008, Institute of Oceanology Polish Academy of Science, Sopot, 244 pp.

Schmidt, B., Wodzinowski, T., Bulczak, A.I., 2021. *Long-term variability of near-bottom oxygen, temperature, and salinity in the Southern Baltic*. J. Marine Syst. 213, 103462.
https://doi.org/10.1016/j.jmarsys.2020.103462

Sharp, J.M., 2002. *Analytical methods for total DOM pools*. [In:] Hansell, D.A., Carlson, C.A., (Eds.), *Biogeochemistry of Marine Dissolved Organic Matter*. Elsevier Science, San Diego, 35–58.

Simis, S.G.H., YloÈstalo, P., Kallio, K.Y., Spilling, K., Kutser, T., 2017. *Contrasting seasonality in optical-biogeochemical properties of the Baltic Sea*. PLoS ONE 12 (4), e0173357.

Stedmon, C.A., Bro, R., 2008. *Characterizing dissolved organic matter fluorescence with parallel factor analysis: a tutorial*. Limnol. Oceanogr. Methods, 6, 572–579.

Stedmon, C.A., Markager, S., 2001. *The optics of chromophoric dissolved organic matter (CDOM) in the Greenland Sea: An algorithm for differentiation between marine and terrestrially derived organic matter*. Limnol. Oceanogr. 46 (8), 2087–2093.

Stedmon, C.A., Markager, S., 2003. *Behaviour of the Optical Properties of Coloured Dissolved Organic Matter Under Conservative Mixing*. Estuar. Coast. Shelf Sci. 57, 973–979.
https://doi.org/10.1016/S0272-7714(03)00003-9

Stedmon, C.A., Markager, S., 2005. *Tracing the production and degradation of autochthonous fractions of dissolved organic matter by fluorescence analysis*. Limnol. Oceanogr. 50 (5), 1415–1426.

Stedmon, C.A., Markager, S., Bro, R., 2003. *Tracing dissolved organic matter in aquatic environments using a new approach to fluorescence spectroscopy*. Mar. Chem. 82 (3–4), 239–254.

Stedmon, C.A., Markager, S., Kaas, H., 2000. *Optical properties and signatures of Chromophoric Dissolved Organic Matter (CDOM) in Danish Coastal waters*. Estuar. Coast. Shelf. Sci. 51, 267–278.

Stedmon, C.A., Markager, S., Tranvic, L., Kronberg, L., Slätis, T., Martinsen, W., 2007. *Photochemical production of ammonium and transformation of dissolved organic matter in the Baltic Sea*. Mar. Chem. 104, 227–240.

Stedmon, C.A., Nelson, N.B., 2015. *Chapter 10 – The optical properties of DOM in the ocean*. [In:] Hansell, D.A., Carlson, C.A. (Eds.), *Biogeochemistry of Marine Dissolved Organic Matter*, 2nd Edn., Acad. Press, Boston,

481–508. https://doi.org/10.1016/B978–0-12–405940–5.00010–8

Stedmon, C.A., Osburn, C.L., Kragh, T., 2010. *Tracing water mass mixing in the Baltic–North Sea transition zone using the optical properties of coloured dissolved organic matter*. Estuar. Coast. Shelf Sci. 87, 156–162. https://doi.org/10.1016/j.ecss.2009.12.022

Terzić, E., Zabłocka, M., Loginova, A.N., Kowalczuk, P., 2024. *Estimation of net and removal of fluorescent dissolved organic matter in different Baltic Sea water masses*. Front. Mar. Sci. 11. https://doi.org/10.3389/fmars.2024.1379604

Vähätalo, A.V., Wetzel, R.G., 2008. *Long-term photochemical and microbial decomposition of wetland-derived dissolved organic matter with alteration of 13C:12C mass ratio*. Limnol. Oceanogr. 53, 1387–1392.

Wagner, S., Schubotz, F., Kaiser, K., Hallmann, C., Waska, H., Rossel, P.E., Hansman, R., Elvert, M., Middelburg, J.J., Engel, A., Blattmann, T.M., Catalá, T.S , Lennartz, S.T., Gomez-Saez, G.V., Pantoja-Gutiérrez, S., Bao, R., Galy, V., 2020. *Soothsaying DOM: A Current Perspective on the Future of Oceanic Dissolved Organic Carbon*. Front. Mar. Sci. 7, 341. https://doi.org/10.3389/fmars.2020.00341

Weishaar, J.L., Aiken, G.R., Bergamaschi, B.A., Fram, M.S., Fujii, R., Mopper, K., 2003. *Evaluation of Specific Ultraviolet Absorbance as an Indicator of the Chemical Composition and Reactivity of Dissolved Organic Carbon*. Environ. Sci. Technol. 37 (20), 4702–4708. https://doi.org/10.1021/es030360x

Xie, H., Aubry, C., Bélanger, S., Song, G., 2014. *The dynamics of absorption coefficients of CDOM and particles in the St. Lawrence estuarine system: Biogeochemical and physical implications*. Mar. Chem. 128. https://doi.org/10.1016/j.marchem.2011.10.001

Yamashita, Y., Tsukasaki, A., Nishida, T., Tanoue, E., 2007. *Vertical and horizontal distribution of fluorescent dissolved organic matter in the Southern Ocean*. Mar. Chem. 106, 498–509.

Zabłocka, M., Kowalczuk, P., Stoń-Egiert, J., Terzić, E., Bournaka, E., Palacz, A.P, 2025. *Tracing theorigins and transformations of fluorescence dissolved organic matter within western and eastern Greenland's shelves: a comparative study*. Front. Mar. Sci. 11. https://doi.org/10.3389/fmars.2024.1476768

Zsolnay, A., Baigar, E., Jimenez, M., Steinweg, B., Saccomandi, F., 1999. *Differentiating with fluorescence spectroscopy the sources of dissolved organic matter in soils subjected to drying*. Chemosphere, 38 (1), 45–50. https://doi.org/10.1016/S0045-6535(98)00166-0